reagent) was added to each well (100 μL/well). The plates were incubated for 1 h at RT and washed three times with washing buffer. Colour was developed by adding 100 μL 3,3′,5,5′-tetramethylbenzidine/urea hydrogen peroxide (Neogen, Lexington, KY, USA) and incubating the plates for 30 min at RT. Colour development was stopped by adding 1 mol/L sulphuric acid (100 μL/well), and the optical density (OD) was measured at 450/640 nm. The optimum reaction conditions were determined in the following ranges: 0.5×10^8 to 3×10^8 vg of AAV-2 vector particles per well, 10- to 5000-fold dilution of the specimen and 0.01–0.4 μg/mL concentration of HRP-IgG. The effects of bilirubin, haemoglobin and chyle as endogenous interference materials were studied. Samples including these materials at 500 mg/L, 5000 mg/L and 3000°, respectively, were mixed with sera at a volume ratio of 1 : 9 and analysed by ELISA.

For the nAb assay, sera were continuously diluted two-fold with Dulbecco's Modified Eagle's Medium and Harn's F-12 Nutrient Mixture (DMEM/F12, Invitrogen) 10% fetal bovine serum (Sigma-Aldrich, St. Louis, MO, USA), 100 U/mL penicillin (Invitrogen) and 100 μg/mL streptomycin (Invitrogen). AAV-2 vectors were diluted with 10 mmol/L HEPES/130 mmol/L NaCl (pH 8.0) up to 1.4×10^8 vg/μL, and optimum transduction was obtained with 1.4×10^{10} vg/μL. Ten microlitres of diluted serum were added to 5 μL diluted AAV-2 vector, and the mixture was incubated for 1 h at RT. The mixture was then added to 96-well plates containing confluent HEK293 cells. Two days after transduction, β-galactosidase activity was measured with a β-galactosidase assay kit (Invitrogen). The titre of nAb was defined as the highest dilution of serum that showed <50% of the β-galactosidase activity of the negative control.

Results and discussion

In the ELISA method developed in this study, AAV-2 vector particles immobilized on plates captured AAV-2-specific antibodies. Using whole vector particles as antigens without degradation, antibodies that are more specific AAV-2, including nAb, can be assessed. Intra-assay precision was determined by repeatedly ($n = 8$) measuring four kinds of serum with different nAb titres. For three samples whose nAb titres were ×640, ×80 and ×80, the coefficient of variation (CV) of the OD was 2.5%, 4.3% and 1.8%, respectively. For the fourth sample, with ×10 titre, the average OD was 0.012 and the CV was 8.5%. These data confirm the good precision of the assay. The effects of interference materials were <10%, suggesting that the method had good specificity. All reagents, including AAV particles, were stable after storage for 13 months at 4°C, and sensitivity of the ELISA was maintained at 95% with fresh reagents.

The nAb titres for 20 healthy donor samples varied from ×10 to ×640, and 13 samples had a titre less than ×20. Using the ELISA method, the absorbance values of the samples varied from 0.012 to 0.752, and 15 samples showed absorbance of less than 0.08 (Table 1). In our study, a nAb titre higher than × 32 corresponded to an OD greater than 0.5 in the ELISA. If these values were used as cut-off points, two of 20 samples found to be positive in both the nAb assay and the ELISA. Further studies on more samples were necessary to validate the cut-off values in different populations.

Table 1 Correlation between a neutralizing antibody assay (nAb) and the ELISA method

	nAb assay		ELISA	
Sample ID	nAb titre	Decision	OD	Decision
1	10	Neg.	0.014	Neg.
2	80	Neg.	0.075	Neg.
3	10	Neg.	0.013	Neg.
4	10	Neg.	0.016	Neg.
5	160	Neg.	0.291	Neg.
6	80	Neg.	0.015	Neg.
7	80	Neg.	0.032	Neg.
8	10	Neg.	0.010	Neg.
9	10	Neg.	0.025	Neg.
10	10	Neg.	0.012	Neg.
11	10	Neg.	0.014	Neg.
12	80	Neg.	0.468	Neg.
13	10	Neg.	0.012	Neg.
14	320	Pos.	0.596	Pos.
15	640	Pos.	0.725	Pos.
16	10	Neg.	0.013	Neg.
17	20	Neg.	0.114	Neg.
18	10	Neg.	0.046	Neg.
19	10	Neg.	0.016	Neg.
20	10	Neg.	0.012	Neg.

OD, optical density; ELISA, enzyme-linked immunosorbent assay; nAb, neutralizing antibodies

AAV-2 antibody in 20 sera from healthy individuals was analysed by ELISA and a neutralizing antibody assay. The measured values were expressed as OD or titre. The cut-off value for the neutralizing antibody assay was provisionally fixed at ×320. The criterion for positivity for the ELISA method was considered greater than OD 0.5

Conclusion

We have developed a simple and convenient ELISA method for detecting serum anti-AAV-2 antibodies. Antibody titres assessed by this method show good correlation with nAb titres obtained in a cell transduction assay, suggesting that this ELISA may be useful for the rapid screening of nAbs in candidates for gene therapy.

DECLARATIONS

Competing interests: None.

Funding: Part of this work was supported by a grant (19591003) from the Ministry of Education, Science, Sports and Culture of the Japanese Government, and a grant (20261501) from the Japan Ministry of Health, Labour and Welfare.

Ethical approval: The ethics committee of Jichi Medical University approved this study (GT-001).

Guarantor: SM.

Contributorship: Conceived and designed the experiments: SM, HM, TI, TH. Performed the experiments: TY, MK, HM, Analysed the data: TI, SY, TH, MK, HM, KO, SM, Wrote the paper: TI, SM.

REFERENCES

1 Gao G, Vandenberghe LH, Alvira MR, *et al.* Clades of adeno-associated viruses are widely disseminated in human tissues. *J Virol* 2004;78:6381–8
2 Wu Z, Asokan A, Samulski RJ. Adeno-associated virus serotypes: vector toolkit for human gene therapy. *Mol Ther* 2006;14:316–27
3 Chirmule N, Propert K, Magosin S, *et al.* Immune responses to adenovirus and adeno-associated virus in humans. *Gene Ther* 1999;6:1574–83
4 Moskalenko M, Chen L, van Roey M, *et al.* Epitope mapping of human anti-adeno-associated virus type 2 neutralizing antibodies: implications for gene therapy and virus structure. *J Virol* 2000;74:1761–6
5 Li XG, Okada T, Kodera M, *et al.* Viral-mediated temporally controlled dopamine production in a rat model of Parkinson disease. *Mol Ther* 2006;13:160–6

(Accepted 24 June 2009)

THE JOURNAL OF GENE MEDICINE
J Gene Med 2009; **11**: 373–381.
Published online 9 March 2009 in Wiley InterScience (www.interscience.wiley.com) **DOI:** 10.1002/jgm.1313

RESEARCH ARTICLE

Retroviral vector-producing mesenchymal stem cells for targeted suicide cancer gene therapy

Ryosuke Uchibori[1]
Takashi Okada[1†]
Takayuki Ito[1]
Masashi Urabe[1]
Hiroaki Mizukami[1]
Akihiro Kume[1]
Keiya Ozawa*[1]

[1]*Division of Genetic Therapeutics, Center for Molecular Medicine, Jichi Medical University, Tochigi, Japan*

*Correspondence to: Keiya Ozawa, Division of Genetic Therapeutics, Jichi Medical University, 3311-1 Yakushiji, Shimotsuke, Tochigi 329-0498, Japan.
E-mail: titou@jichi.ac.jp

†Present address: Department of Molecular Therapy, National Institute of Neuroscience, National Center of Neurology and Psychiatry, Tokyo, Japan.

Received: 30 May 2008
Revised: 31 October 2008
Accepted: 19 January 2009

Abstract

Background Mesenchymal stem cells (MSCs) are a promising vehicle for targeted cancer gene therapy because of their potential of tumor tropism. For efficient therapeutic application, we developed retroviral vector-producing MSCs that enhance tumor transduction via progeny vector production.

Methods Rat bone marrow-derived MSCs were nucleofected with the proviral plasmids (vesicular stomatitis virus-G protein-pseudotyped retroviral vector components) (VP-MSCs) or pLTR plasmid alone (non-VP-MSCs). The luciferase-based *in vivo* imaging system was used to assess gene expression periodically. To evaluate the anticancer effects, we administered MSCs expressing herpes simplex virus-thymidine kinase (HSV-*tk*) into the left ventricular cavity of nude mice engrafted with 9L glioma cells subcutaneously.

Results *In vivo* imaging revealed that administration of luciferase-expressing non-VP-MSCs enhanced the bioluminescence signal at the inoculation sites of 9L cells, whereas no accumulation was observed in mice at the site of the control Rat-1 fibroblasts. Compared to non-VP-MSCs, the administration of VP-MSCs resulted in significant augmentation of the signal with an increase in transgene copy number. Immunohistochemical analysis showed marked luciferase expression at the tumor periphery in mice injected with VP-MSCs, whereas little expression was detected in those injected with non-VP-MSCs. Under the continuous infusion of ganciclovir, systemic administration of VP-MSCs expressing HSV-*tk* suppressed tumor growth more effectively than non-VP-MSC administration, whereas no anticancer effect was observed without ganciclovir treatment. Furthermore, VP-MSC administration caused no transgene transduction in the normal tissues and organs.

Conclusions VP-MSCs accumulated at the site of tumors after intravascular injection in tumor-bearing mice, followed by *in situ* gene transfer to tumors without transduction of normal organs. When applied to the HSV-*tk*/ganciclovir suicide gene therapy, more efficient tumor growth suppression was observed using VP-MSCs compared to non-VP-MSCs. This VP-MSC-based system has great potential for improved cancer gene therapy. Copyright © 2009 John Wiley & Sons, Ltd.

Keywords HSV-*tk*; in vivo imaging; retroviral vector; suicide cancer gene therapy; vector-producing MSCs

Introduction

Tumor invasions and metastases are the principal causes of death in patients with cancer. However, current anticancer strategies are typically associated with high toxicity and modest success rates. Suicide gene therapy has been tested for the treatment of invasive tumors such as malignant glioma; for this

therapy, retroviral vectors expressing herpes simplex virus-thymidine kinase (HSV-*tk*) combined with treatment with the prodrug ganciclovir (GCV) have been developed [1]. However, this system still has two hurdles, namely, the transduction efficiency of tumors and immune responses generated against the vectors [2]. In addition, it is essential that the vector has a tumor tracking property to effectively attack invasive or metastatic lesions with minimal adverse effects [3].

Mesenchymal stem cells (MSCs), as derived from adult bone marrow, fat, or fetal tissues, are a promising tool for regenerative medicine because of their self-renewal capacity and multilineage differentiation ability. Recent evidence suggests that bone marrow-derived MSCs selectively accumulate at tumors, and they are promising vehicles for tumor-targeting therapy [4,5]. However, MSCs may provide structural support to malignant cells and locally attenuate the tumor surveillance system through their immunosuppressive effects, leading to the progression of tumor growth [6–8]. Therefore, MSCs should be modified to have an increased antitumor activity in order to use them for cancer gene therapy [5,9,10].

Systemic administration of genetically modified MSCs to produce an anticancer cytokine has been shown to be effective in tumor suppression. Intravenous injection of MSCs expressing interferon (IFN)-β inhibits the expansion of the pulmonary metastasis of melanoma and breast cancer in mice [11] and prolongs the survival of mice with glioma xenografts [4]. For more efficient and specific MSC-based gene therapy, we aimed to develop MSCs with a vector-producing property.

In the present study, we developed MSCs that locally produce the HSV-*tk*-expressing retroviral vectors (VP-MSCs), which facilitate transgene transduction and tumor targeting. By using a mouse subcutaneous glioma model, we examined tumor tropisms and cancer-killing effects of systemically administered VP-MSCs. To assess the safety of this system, we demonstrated that tumor-specific transduction was achieved by the progeny retroviruses produced by VP-MSCs at the site of tumors.

Materials and methods

Cell culture

The malignant rat glioma cell line 9L and fibroblasts derived from a normal rat Rat-1 were obtained from the Riken BRC Cell Bank (Ibaraki, Japan) [12]. The stable firefly luciferase-expressing rat MSCs and 9L (9L/LNCL) were developed by transduction with a recombinant retroviral vector encoding luciferase and neomycin resistance genes. The cells were cultured in Dulbecco's modified Eagle's medium and nutrient mixture F12 (DMEM-F12; Invitrogen, Grand Island, NY, USA) and 10% fetal bovine serum (FBS; Sigma Chemical Co., St Louis, MO, USA) supplemented with 100 units/ml of penicillin and 100 μg/ml of streptomycin in an atmosphere of 5% CO_2 at 37 °C.

MSC isolation and culture

All animal experiments were approved by the Jichi Medical University ethics committee and were performed in accordance with the National Institutes of Health Guide for the Care and Use of Laboratory Animals. MSCs were prepared from the rat bone marrow as described previously [13]. Briefly, 5-week-old male Sprague-Dawley (SD) rats (Clea Japan, Tokyo, Japan) were sacrificed by an overdose of isoflurane inhalation, and their femurs and tibias were dissected. After the epiphyses were removed, the bone marrow was flushed out with DMEM-F12. A single cell suspension was obtained by sequential drawing of the marrow into syringes through 27-G needles. The cells were cultured at a density of 1×10^6 cells/cm^2 in noncoated T-25 or T-75 cell culture flasks containing DMEM-F12 and 10% FBS supplemented with 100 units/ml of penicillin and 100 μg/ml of streptomycin in an atmosphere of 5% CO_2 at 37 °C. After 3 or 4 days of culture, the medium was replaced and the non-adherent cells removed. Thereafter, the medium was then changed twice weekly. When 60–80% confluence was attained, the adherent cells were placed at a density of 1×10^4 cells/cm^2 in a T-225 flask for expansion. After 15 passages, the cells were used for the experiments.

VP- and non-VP-MSC preparation

HSV-*tk* or the firefly luciferase expression cassette was cloned into pLTR to create pLTR-*tk* or pLTR-*luc*. pGP and pVSV-G express the Moloney murine leukemia virus gag-pol and the vesicular stomatitis virus-G (VSV-G) pseudotyped envelope protein under the control of a cytomegalovirus promoter, respectively [12]. Nucleofection of MSCs was performed according to the manufacturer's instructions (Amaxa Biosystem, Cologne, Germany). To generate VP-MSCs, 2×10^6 MSCs were gently resuspended in 100 μl of Human Mesenchymal Nucleofector Solution (Amaxa Biosystem) and mixed with the proviral plasmids pGP, pVSV-G and pLTR-*tk* or pLTR-*luc* at concentrations of 1, 1 and 2 μg, respectively. The mixture was then pulsed with the program U-23. Non-VP-MSCs were generated by nucleofection with pLTR-*tk* or pLTR-*luc* alone. Vector-producing HEK293 (VP-293) cells and non-VP-293 cells were similarly developed by nucleofection using the X-01 pulse program. Cells were cultured in six-well plates containing prewarmed DMEM-F12 before the experiments. Quantification of RNA genome titer in culture supernatant was determined by reverse transcription-quantitative polymerase chain reaction (PCR) using a Retrovirus Titer Set (Takara Bio Inc., Shiga, Japan) according to the manufacturer's instructions. The results of viral titer were expressed as genomes/μl.

Transduction of 9L cells and MSCs with progeny retrovirus produced by VP-MSCs

The 100-μl culture supernatants of luciferase-expressing VP-MSCs or non-VP-MSCs in a 96-well plate after 24 h of nucleofection were added to 9L cells or MSCs (1×10^4 cells for each well) in a 96-well plate. After 48 h of incubation, transduction efficiency was estimated by the luciferase assay using a chemiluminometer (Fluoroskan Ascent FL, Thermo Labsystem, Beverly, MA, USA) and the Bright-Glo Reagent kit (Promega, Madison, WI, USA) according to the manufacturer's instructions.

Chemiluminescence assay for evaluating tumor-killing effects *in vitro*

9L/LNCL cells stably expressing luciferase were used in the present study. Briefly, 5×10^4 9L/LNCL cells were cocultured with 2.5×10^4 VP-MSCs or non-VP-MSCs in 48-well flat-bottomed plates (day 0). At day 3, the cells were exposed to varying concentrations (0.01–100 μmol/l) of GCV (F. Hoffmann-La Roche, Basel, Switzerland). At day 7, the luciferase assay was performed with a chemiluminometer (Thermo Labsystem) using the Bright-Glo Reagent kit (Promega) according to the manufacturer's instructions.

Determination of HSV-tk transgene copy number *in vitro*

To estimate the copy number of transgene in the cells transduced with retroviral progeny, 9L cells and MSCs were co-cultured and whole cells were collected at day 7. Quantitative values were obtained from the threshold cycle (Ct) number that indicated exponential amplification of the PCR product by using a sequence detection system (ABI Prism 7700; Applied Biosystems, Madison, WI, USA). The relative copy number of the HSV-*tk* gene was determined as the ratio of the copy numbers in the group of 9L cells co-cultured with VP-MSCs to the copy numbers in the non-VP-MSC group. The copy number of the reference gene *GAPDH* was also determined to correct the variation in the DNA amount and amplification efficiency. The gene specific primers are shown below: HSV-*tk* forward, 5′-CGTCGCCGATGGGGTGTTCT-3′, reverse, 5′-GCGCGGCCGGGTAGCACAGG-3′, rat *GAPDH* forward, 5′-CAGCAATGCATCCTGCAC-3′, and reverse, 5′-GAGTTGC-TGTTGAAGTCACAGG-3′.

In vivo bioluminescence imaging for detecting transgene expression

9L cells or Rat-1 cells (3×10^6 each) in 100 μl of phosphate buffer saline (PBS) containing 25% (v/v) basement membrane matrix (Matrigel; BD Biosciences, Franklin Lakes, NJ, USA) were subcutaneously inoculated into the bilateral dorsal region (3×10^6 cells/site) of 4- to 6-week-old male Balb/c nu/nu mice (Clea Japan). Immediately after inoculation, the luciferase-expressing VP-MSCs or non-VP-MSCs (5×10^5 cells/body each) were injected into the left ventricular cavity of mice. Three experimental groups were formed: group 1, mice inoculated with Rat-1 cells and injected with non-VP-MSCs; group 2, mice inoculated with 9L cells and injected with non-VP-MSCs; and group 3, mice inoculated with 9L cells and injected with VP-MSCs; $n = 4$ for each group. After injection of the cells, optical bioluminescence imaging was performed to periodically trace the cells using an *in vivo* imaging system (IVIS; Xenogen, Hopkinton, MA, USA). The reporter substrate D-luciferin (75 mg/kg body weight) was injected into the mouse peritoneum for scanning. The luminescence levels in the region of interest (total flux; photons/sec) were analysed using the Living Image software (Xenogen, Alameda, CA, USA).

Immunohistochemistry

Mice were anesthetized with an overdose of isoflurane inhalation and fixed by perfusion with 4% paraformaldehyde. The tissues were then embedded in an optimal cutting temperature compound (Sakura Finetek, Tokyo, Japan), frozen, and sectioned into 20-μm-thick slices. Immunohistochemical staining was performed with a rabbit monoclonal anti-luciferase antibody (1 : 5000; Promega) by the avidin-biotin-peroxidase method. Irrelevant rabbit immunoglobulin (Ig)G (Promega) was used as a negative control. Sections were treated with horseradish peroxidase-labelled anti-rabbit IgG secondary antibody (Dako, Glostrup, Denmark; 1 : 200), and luciferase-positive cells were visualized using the Vectastain Elite ABC kit (Vector Laboratories, Burlingame, CA, USA). The sections were counterstained with hematoxylin.

Determination of luciferase transgene copy number *in vivo*

To estimate the copy number of transgene in tissues in tumor-bearing mice, small pieces of tissues were obtained from peripheral and central portions of the tumors at 21 days after MSC administration. Quantitative values were obtained from the threshold cycle (Ct) number that indicated exponential amplification of the PCR product by using the sequence detection system (ABI Prism 7700). The relative copy number of the *luciferase* gene was determined as the ratio of the copy numbers in the peripheral or central portions of tumors in the group of 9L tumor in mice inoculated with VP-MSCs to the copy numbers in non-VP-MSCs group. The copy number of the reference gene *GAPDH* was also determined to correct for variation in the DNA amount

and amplification efficiency. The gene specific primers were: *Luc* forward, 5′-TTCTGGGGGCGCACCTCTTC-3′, and reverse, 5′-GGGGGCCACCTGATATCCTTTGTA-3′.

Survival of MSCs at the tumor sites *in vivo*

The stable luciferase-expressing MSCs were mixed with an equal number of nontransduced 9L cells (1.5×10^6 cells each) and were suspended in 100 µl of PBS containing 25% (v/v) Matrigel. Immediately, the mixture was subcutaneously inoculated into the bilateral dorsal region of nu/nu mice ($n = 4$ for each group). Luminescence at the tumor sites was periodically determined using IVIS (Xenogen), and the luminescence levels were analysed using Living Image software (Xenogen).

Assessment of tumor-specific transduction

To estimate the level of progeny retroviral transduction, PCR analysis was performed. DNA was extracted from the tumors or normal tissues by using a DNA extraction kit (Qiagen) at 21 days after MSC injection and then amplified using Ex Taq (Takara Bio Inc.). The PCR products (560 bp) extending from the 5′ long-terminal repeat (LTR) or 3′-LTR of the retroviral vector were produced using the gene-specific primers: LTR forward, 5′-AGGGCCAAGAACAGATGAGACAGC-3′ and reverse, 5′-GTACAGACGCAGGCGCATAACATC-3′. Conversion of the 3′-LTR to the 5′-LTR after retroviral transduction was confirmed by the typical banding pattern (440 bp + 120 bp fragments) generated after *Xba*I digestion.

Assessment of the anticancer effects of VP-MSCs *in vivo*

9L/LNCL cells (3×10^6 each) in 100 µl of PBS containing 25% (v/v) Matrigel were subcutaneously inoculated in the bilateral dorsal region of 4- to 6-week-old male Balb/c nu/nu mice. PBS (group 1), MSCs (group 2), HSV-tk-expressing non-VP-MSCs (group 3) or VP-MSCs (group 4; 5×10^5 cells/body each) were then injected into the left ventricular cavity of the mice ($n = 4$ for each group). Seven days after MSC injection, GCV (100 mg/kg/day) or PBS was continuously administered into the peritoneum by using mini-osmotic pumps (Alzet, Palo Alto, CA, USA) for 28 days. The tumor growth was monitored two or three times a week by measuring tumor sizes using a caliper, and tumor volumes were calculated using the formula: tumor volume (mm^3) = $a(mm) \times b^2(mm^2) \times 0.5$ (a, the height of the tumor; b, the width of the tumor).

Statistical analysis

Data from multiple experiments are expressed as the mean ± SEM. Statistical analyses were performed using StatView (Abacus Concepts, Inc., London, UK). Differences in parameters were evaluated by analysis of variance combined with Welch's t-test. $p < 0.05$ was considered statistically significant.

Results

Characterization of VP-MSCs

Consistent with previous studies, the bone marrow-derived rat MSCs used in the present study exhibited a spindle shape; they differentiated into adipocytes, osteocytes, and chondrocytes in appropriate culture media (data not shown). The green fluorescence protein (GFP)-based semiquantitative analysis revealed that nucleofection is more efficient for the transfection of MSCs than the calcium-phosphate method and lipofection: the percentage of GFP-positive MSCs after 24 h of transfection by each method was approximately 60.1%, 3.1% and 12.3%, respectively.

The secretion of retroviral vectors into the culture media of VP-MSCs (Figure 1a) and VP-293 cells (Figure 1b) increased and peaked at 48 h after nucleofection, whereas the vector production from non-VP-MSCs or non-VP-293 cells was undetectable. There was no significant difference in the amounts of produced vectors at 48 h between VP-MSCs and VP-293 cells.

Chemiluminescence assay showed that 9L glioma cells were efficiently transduced with the vectors generated from VP-MSCs (Figure 1c). On the other hand, when MSCs were treated with the culture media of VP-MSCs or non-VP-MSCs, transduction was undetectable (Figure 1d).

Tumor-killing effects of VP-MSCs *in vitro*

The *in vitro* luciferase assay revealed that the bioluminescence signal of luciferase-expressing 9L/LNCL cells decreased in a GCV dose-dependent manner after coculture with HSV-*tk*-expressing MSCs (Figure 1e). The concentration required to induce a 50% inhibition (IC_{50}) value of GCV in the presence of VP-MSCs at day 7 was considerably lower than that in the presence of non-VP-MSCs (0.33µmol/l versus 83µmol/l). At this time-point, real-time PCR analysis showed that the relative copy number of the HSV-*tk* gene in the VP-MSC group was approximately 17.5-fold more than that in the non-VP-MSC group (Table 1). Because transduction of MSCs with progeny retrovirus was inefficient (Figure 1d), these data suggests that 9L glioma cells were mainly transduced with progeny luciferase-expressing retrovirus produced by VP-MSCs (Figure 1c).

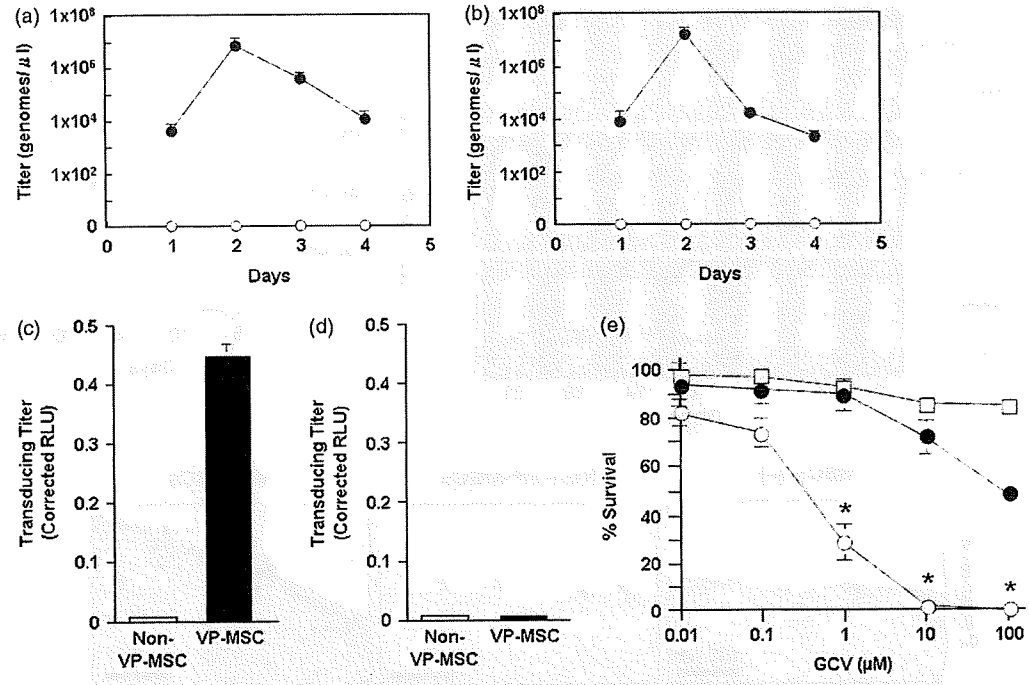

Figure 1. Function of vector-producing mesenchymal stem cells (VP-MSCs) *in vitro*. (a, b) Time course of luciferase-expressing retrovirus production from VP-MSCs and vector-producing HEK293 (VP-293) cells. VP-MSCs (a, ●; $n = 3$) or VP-293 (b, ●; $n = 3$) were developed with pGP, pVSV-G, and pLTR-*luc* at concentrations of 1, 1 and 2 μg by nucleofection. Non-VP-MSCs (a, ○; $n = 3$) or non-VP-293 (b, ○; $n = 3$) were developed with pLTR-*luc* by nucleofection. The RNA genome titer of progeny virus in the culture supernatant of these cells was determined by reverse transcription-quantitative PCR. (c, d) Transduction of rat glioma 9L cells (c) or MSCs (d) with luciferase-expressing retrovirus produced by VP-MSCs. The 9L cells and MSCs were treated with the culture supernatant of non-VP-MSCs (open bar; $n = 3$) or VP-MSCs (solid bar; $n = 3$) that were nucleofected 2 days before. The luminescence levels of these cells were measured by a chemiluminescence luciferase assay after 48 h of treatment. (e) Tumor-killing effects of VP-MSCs *in vitro*. MSCs were cocultured with luciferase-expressing 9L/LNCL glioma cells at a ratio of 1 : 3 (day 0), and different doses of GCV (0.01–100 mmol/l) were added to the culture media on day 3. The number of viable 9L/LNCL cells was estimated by a luciferase assay on day 7. The groups were as follows: MSCs without genetic modification (□); MSCs nucleofected with herpes simplex virus-thymidine kinase (HSV-*tk*)-expressing plasmid (non-VP-MSCs, ●); and MSCs nucleofected with retroviral vector components pLTR-*tk*, pGag-pol, and pVSV-G (VP-MSCs, ○). For each group, $n = 3$; $^*p < 0.05$ versus non-VP-MSC group

Table 1. Relative HSV-*tk* transgene copy number in the co-cultures of 9L tumor cells and MSCs

	Relative HSV-*tk* transgene copy number
Non-VP-MSCs	1.0
VP-MSCs	17.5

9L cells and MSCs were co-cultured and whole cells were collected at day 7. The relative copy number of the HSV-*tk* gene was determined as the ratio of the copy numbers in the group of 9L cells co-cultured with VP-MSCs to the copy numbers in the non-VP-MSC group. The copy number of the reference gene *GAPDH* was also determined to correct the variation in the DNA amount and amplification efficiency.

Tumor tropism of VP-MSCs *in vivo* and enhanced transgene expression *in situ*

In vivo imaging indicated that luciferase-expressing MSCs transiently appeared just after injection at high perfusion organs, such as the brain, liver, kidney and spleen, irrespective of administration of VP- or non-VP-MSCs (day 0). After systemic administration of non-VP-MSC, the signal peaked at day 10 and declined thereafter at the tumor sites, whereas no signal enhancement was observed at the site of Rat-1 inoculation (Figures 2a and 2b). By contrast, the signal after administration of VP-MSCs further increased over day 21 (Figures 2c and 2d), and no signal was observed in the normal organs at this time-point. Immunohistochemical studies showed marked luciferase expression at the tumor periphery in the VP-MSC group after 21 days of administration (Figure 2e). No signal of luciferase expression was observed in the normal tissues at this time-point. Real-time PCR analysis revealed that the relative copy number of the luciferase gene at the tumor periphery of the VP-MSC group was approximately 47.5-fold more than that of the non-VP-MSC group (Table 2). These results indicate not only successful retroviral vector production by VP-MSCs, but also effective gene transfer by progeny retrovirus *in situ*.

Survival of MSCs at the tumor site

The enhanced signal observed in the VP-MSC group may be in part due to expansion or division of VP-MSCs *in situ*. To exclude this possibility, we estimated the survival of MSCs in the vicinity of the 9L tumor. We employed stable luciferase-expressing MSCs to avoid the conditions of transient gene expression. When the cells were inoculated with 9L tumor cells at the dorsal region

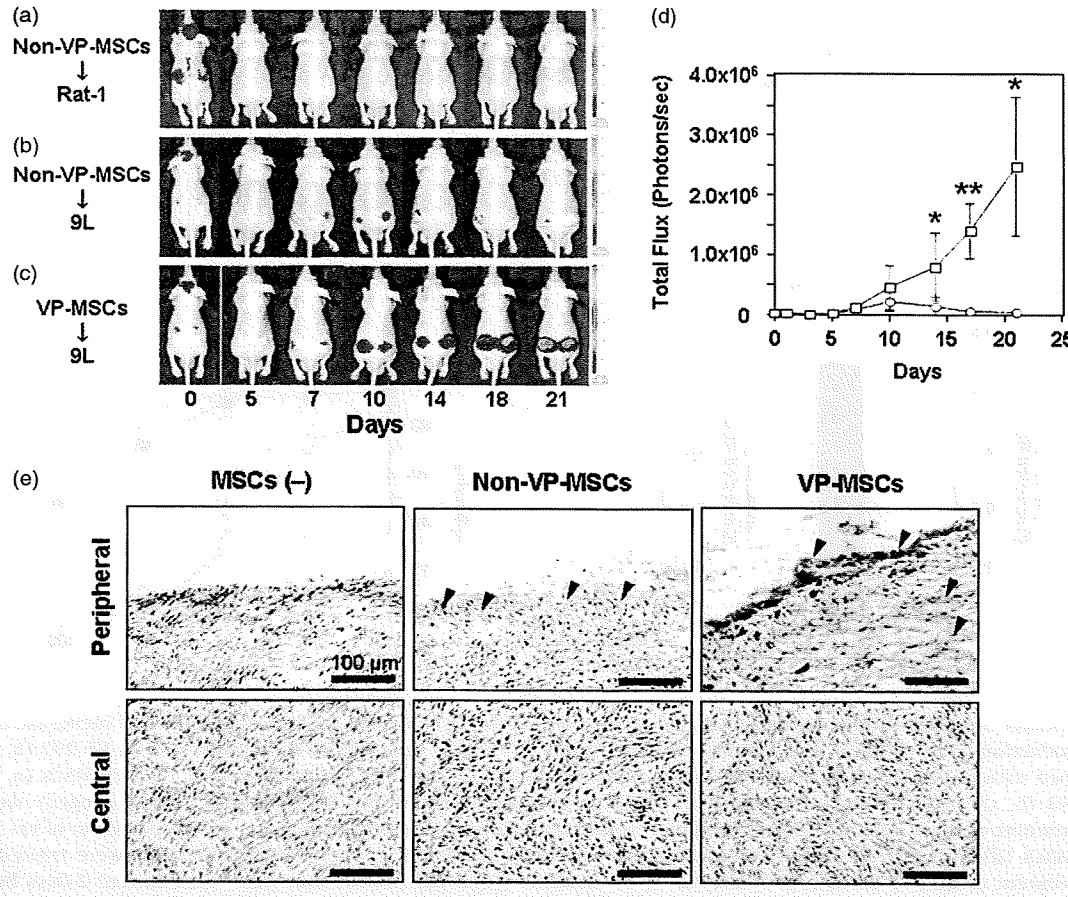

Figure 2. Tumor tropism and enhanced transgene expression after VP-MSC administration. Rat-1 fibroblasts (a) or 9L glioma cells (b, c) were subcutaneously inoculated into the bilateral dorsal region of Balb/c nu/nu mice (3×10^6 cells/site). Luciferase-expressing MSCs (5×10^5 cells/body) were then administered through the left ventricular cavity (day 0). Luminescence was periodically measured through an intraperitoneal injection of D-luciferin (days 0–21). (d) Quantification of luminescence levels at the 9L tumor site after injection of VP-MSCs (□) or non-VP-MSCs (○). For each group, $n = 4$; $^*p < 0.05$ or $^{**}p < 0.01$ versus non-VP-MSC group. (e) Immunostaining for luciferase expression in the subcutaneous tumor. MSCs (5×10^5 cells/body) were injected into the left ventricular cavity immediately after subcutaneous inoculation of 9L cells in the bilateral dorsal part of the Balb/c nu/nu mice (day 0). The tumor tissues were obtained 21 days after MSC administration. Luciferase-positive cells (brown) were detected at the tumor periphery with an anti-luciferase antibody. Arrowheads, luciferase-positive cells. Scale bar = 100 mm

Table 2. Relative *luciferase* transgene copy number in 9L tumors in mice inoculated with VP-MSCs

		Relative *luciferase* transgene copy number	
		Experiment 1	Experiment 2
Central	Non-VP-MSCs.Luc	ND	ND
	VP-MSCs.Luc	ND	ND
Peripeheral	Non-VP-MSCs.Luc	1.0	1.0
	VP-MSCs.Luc	47.5	27.7

Small pieces of tissues were obtained from peripheral and central portions of tumors at 21 days after MSC administration. The relative copy number of the *luciferase* gene was determined as the ratio of the copy numbers in the peripheral portions of tumor in the group of 9L tumors inoculated with VP-MSCs to the copy numbers in non-VP-MSCs. The copy number of the reference gene *GAPDH* was also determined to correct for variation in the DNA amount and amplification efficiency.

of the mice (day 0), the luciferase expression peaked at day 10 and rapidly declined after day 14 (Figures 3a and 3b), indicating the elimination of inoculated MSCs. These results suggest that the signal enhancement after day 14 in the VP-MSC group was not caused by the expansion of inoculated MSCs.

Tumor-specific transduction by VP-MSCs

We evaluated the progeny retroviral transuduction of the tissues at 21 days after MSC administration. The 5′-LTR sequence of transgene in VP-MSCs and non-VP-MSCs does not contain the *Xba*I site (Figure 4a, upper panel). On the other hand, the 5′-LTR sequence of transgene in target cells transduced with progeny retrovirus produced from VP-MSCs contains the *Xba*I site because this 5′-LTR is the copy of 3′-LTR (containing the *Xba*I site) in retroviruses (Figure 4a, lower panel). Therefore, the presence of two fragments (440 bp + 120 bp) of PCR products from the 5′-LTR region (560 bp) indicates that retroviral vector-mediated gene transfer occurred. Because the PCR products from the tumors in the VP-MSC group were digested into two fragments with *Xba*I (Figure 4b), ths means that the tumors were transduced with progeny

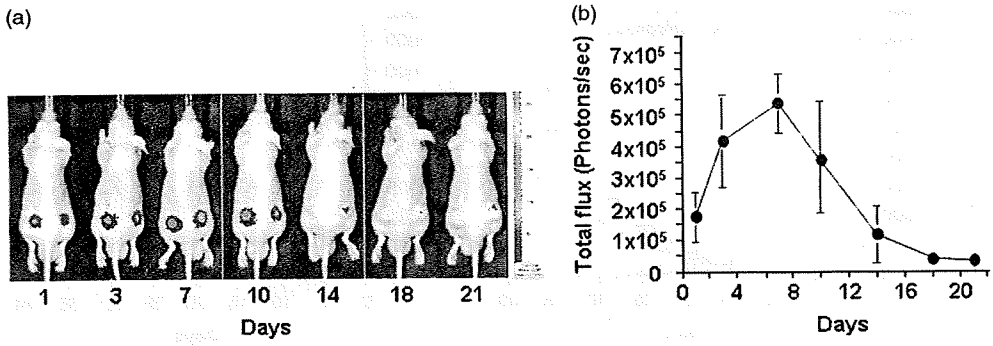

Figure 3. Survival of MSCs in subcutaneous 9L tumor. (a) Typical luminescence signals of luciferase-expressing MSCs measured using an *in vivo* imaging system. Stable luciferase-expressing MSCs mixed with an equal number of nontransduced 9L cells were subcutaneously inoculated into the bilateral dorsal region of nu/nu mice. (b) Time course of the quantified luminescence levels at tumor sites of the mice ($n = 4$)

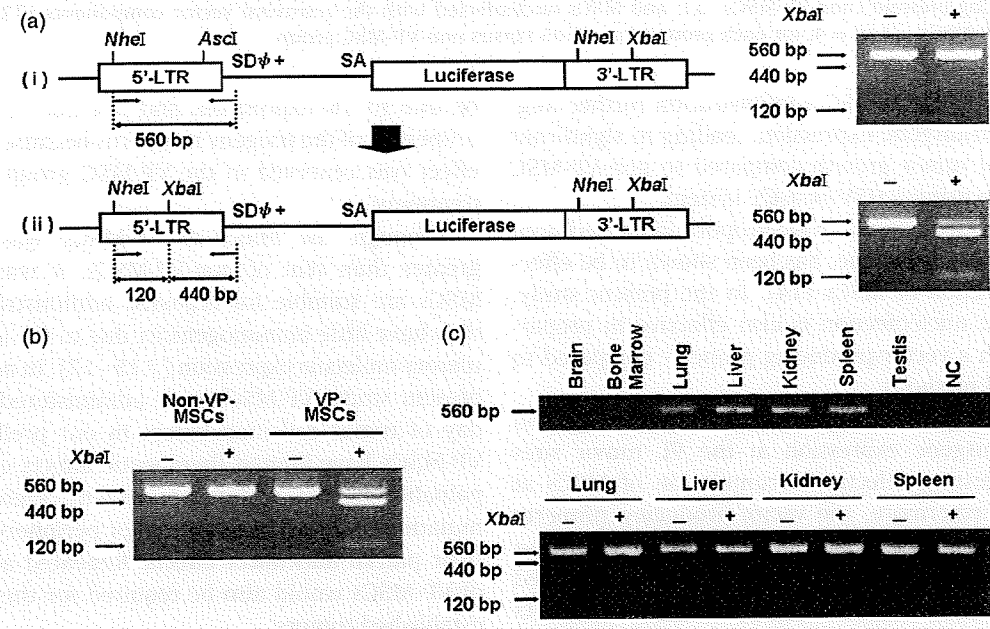

Figure 4. Tumor-specific transduction with progeny retroviral vectors in the VP-MSC system. (a) The diffrence in 5′-LTR sequences between MSCs (VP- and non-VP-) and target cells transduced with progeny retroviruses produced from VP-MSCs. The 5′-LTR sequence of transgene in VP-MSCs and non-VP-MSCs does not contain the *Xba*I site. On the other hand, the 5′-LTR sequence of transgene in target cells transduced with progeny retrovirus produced from VP-MSCs contains the *Xba*I site because this 5′-LTR is the copy of 3′-LTR (containing the *Xba*I site) in retroviruses. Therefore, the presence of two fragments (440 bp + 120 bp) after *Xba*I digestion of PCR products from the 5′-LTR region (560 bp) indicates that retroviral vector-mediated gene transfer occurred. (b) *Xba*I digestion pattern of the PCR products from the 5′-LTR region of the transgene in the tumor periphery at 21 days after MSC administration. The typical *Xba*I digested pattern indicates that transduction of the tumors with progeny retroviruses occurred. (c) The 5′-LTR region in the host tissues was examined by PCR/*Xba*I digestion at day 21 (upper panel). No typical *Xba*I digested pattern was observed in the normal tissues (lower panel), indicating the absence of retroviral vector-mediated gene transfer

retroviruses. In addition, normal tissues in the VP-MSC group were also examined PCR/*Xba*I digestion. Although the 5′-LTR region was amplified in several normal tissues (Figure 4c, upper panel), no typical *Xba*I digested pattern was observed, suggesting that gene transfer did not occur in such normal tissues/organs (Figure 4c, lower panel).

Anticancer effects of VP-MSCs *in vivo*

During the continuous infusion of GCV, tumor growth was significantly suppressed in the VP-MSC group compared to that in the non-VP-MSC, untransfected MSC or non-MSC control groups (Figure 5a). No difference in the tumor growth was observed without GCV administration (Figure 5b).

Discussion

In the present study, we developed MSCs that produce progeny retroviral vectors locally, which enable enhanced and tumor-specific transduction. Systemic delivery of modified MSCs enhanced transgene expression in the

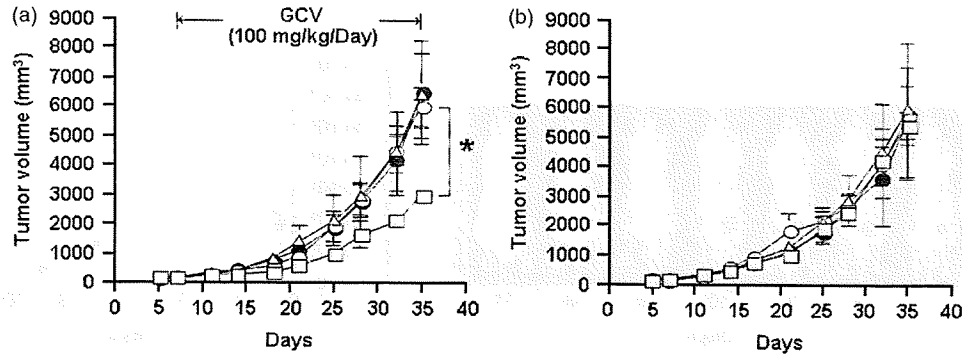

Figure 5. Anticancer effects of VP-MSCs *in vivo*. (a) Suppression of tumor growth after VP-MSC administration under GCV treatment. MSCs were injected into the left ventricular cavity immediately after subcutaneous inoculation of 9L cells into the bilateral dorsal region of Balb/c nu/nu mice (day 0). The mice were continuously administered GCV (100 mg/kg/d) from days 7–35 through intraperitoneal osmotic pumps. The tumor volume was measured periodically. (b) No change was observed in tumor growth without GCV treatment. The groups were: no MSCs (○); MSCs without genetic modification (●); MSCs nucleofected with an HSV-*tk*-expressing plasmid (non-VP-MSCs, Δ); and MSCs nucleofected with the retroviral vector components pLTR-*tk*, pGag-pol, and pVSV-G (VP-MSCs, □) ($n = 4$, for each group). $^*p < 0.05$ versus non-VP-MSC group

9L tumors in mice. VP-MSC administration further augmented local transgene expression, leading to significant suppression of tumor growth compared to non-VP-MSC administration using a HSV-*tk*/GCV system.

Recently, nucleofection, an electroporation-based nonviral transfection technique, has been shown to be effective in transfection of MSCs [14]. In the present study, we found that nucleofection is also effective in preparing MSCs with a vector-producing property compared to other nonviral methods.

We demonstrated that systemic MSC administration enhanced transgene expression at the 9L tumor sites in mice, suggesting selective accumulation of MSCs at the tumor. Furthermore, the vector-producing property augmented amplification and expression of the luciferase gene *in vivo*. Immunostaining studies have demonstrated marked production of the luciferase protein at the tumors in the VP-MSC group. These results suggest that VP-MSCs can locally produce substantial amount of recombinant proteins not only through their homing ability, but also through the enhancement of transgene amplification and expression.

Our results may raise an important question about the origin of bioluminescence and immunostaining signals in the late phase: are the signals derived from VP-MSCs or transduced 9L cells? We demonstrated that most MSCs in the vicinity of 9L glioma cells were eliminated within 14 days *in vivo*. On the other hand, administration of VP-MSCs, but not non-VP-MSCs, further augmented the transgene expression at the tumor site after 14 days. These results suggest that luciferase signals in glioma at day 21 were mainly derived from 9L tumor cells transduced with progeny retroviral vectors.

The GCV-dependent anticancer effect and *tk* gene amplification in the VP-MSC group was significantly greater than that in the non-VP-MSC group *in vitro*. The IC_{50} value of GCV when it was used in concert with VP-MSCs was far lower (approximately 1 : 250) than when it was used with non-VP-MSCs. This anticancer effect of HSV-*tk*-expressing VP-MSCs *in vivo* was considered to be due to TK expression, and not due to the oncolytic properties of the progeny retrovirus because no anticancer effect was observed in the VP-MSC group without GCV treatment.

Although the effect of VP-MSCs was significantly greater than that of non-VP-MSCs, it was still partial. MSCs are suitable for repeated administration because they have little immunogenicity due to the lack of costimulatory molecule expression [7,15–17]. In addition, in the present study, VP-MSCs were administered on the same day of tumor cell inoculation. In our preliminary data, VP-MSCs have limited therapeutic effects on established palpable 9L tumor (data not shown). Preferential accumulation of VP-MSCs at the tumor periphery may explain their partial anticancer effects. Repeated administration of VP-MSCs would also be required for the treatment of established tumors.

Finally, we assessed the biodistribution and replication of progeny retrovirus to ensure the safety and specificity of our system. In the present study, after 21 days of systemic VP-MSC administration, PCR analysis revealed weak amplification of a 5′-LTR sequence in the bone marrow, lungs, kidneys and spleen. When the non-VP- and VP-MSCs were inoculated into the tumor-bearing mice, an IVIS imaging study showed that definite gene expression from MSCs was limited to the tumor site (Figures 2b and 2c). VP-MSCs expressing HSV-*tk* are considered to localize to tumor tissues in the same way. Although a small amount of transgene was detected in several normal tissues by PCR analysis, the *Xba*I-digestion pattern revealed that the transgene was derived from inoculated MSCs (Figure 4c). These results indicate that, even if a small number of injected VP-MSCs were remained in normal tissues, transduction by progeny retrovirus did not occur in these normal tissues. On the other hand, the PCR/*Xba*I digestion experiments showed that retrovirus-mediated gene transfer occurred in the vicinity of tumors. These results ensure the safety and tumor-specific transduction of the VP-MSC system.

In conclusion, this is the first study to demonstrate the effectiveness and safety of systemic administration of VP-MSCs in tumor-bearing mice. VP-MSCs exert their function through *in situ* retroviral vector production and expression of transgenes after accumulation at tumors. Although our system needs to be improved further, the present findings will contribute to the development of more efficient cancer gene therapy using MSCs as a platform.

Acknowledgements

We wish to thank Dr Masafumi Onodera for providing pLTR, pGP and pVSVG. This study was supported in part by Grants-in-aid for Scientific Research; a grant from the 21st Century COE Program; the 'High-Tech Research Center' Project for Private Universities, matching fund subsidy from the Ministry of Education, Culture, Sports, and Technology of Japan; and the Inoue Enryo Memorial Foundation for Promoting Science.

References

1. Ram Z, Culver KW, Oshiro EM, *et al.* Therapy of malignant brain tumors by intratumoral implantation of retroviral vector-producing cells. *Nat Med* 1997; **3**: 1354–1361.
2. Rainov NG. A phase III clinical evaluation of herpes simplex virus type 1 thymidine kinase and ganciclovir gene therapy as an adjuvant to surgical resection and radiation in adults with previously untreated glioblastoma multiforme. *Hum Gene Ther* 2000; **11**: 2389–2401.
3. Hall B, Dembinski J, Sasser AK, *et al.* Mesenchymal stem cells in cancer: tumor-associated fibroblasts and cell-based delivery vehicles. *Int J Hematol* 2007; **86**: 8–16.
4. Nakamizo A, Marini F, Amano T, *et al.* Human bone marrow-derived mesenchymal stem cells in the treatment of gliomas. *Cancer Res* 2005; **65**: 3307–3318.
5. Ozawa K, Sato K, Oh I, *et al.* Cell and gene therapy using mesenchymal stem cells (MSCs). *J Autoimmun* 2008; **30**: 121–127.
6. Karnoub AE, Dash AB, Vo AP, *et al.* Mesenchymal stem cells within tumour stroma promote breast cancer metastasis. *Nature* 2007; **449**: 557–563.
7. Maitra B, Szekely E, Gjini K, *et al.* Human mesenchymal stem cells support unrelated donor hematopoietic stem cells and suppress T-cell activation. *Bone Marrow Transplant* 2004; **33**: 597–604.
8. Hanahan D, Weinberg RA. The hallmarks of cancer. *Cell* 2000; **100**: 57–70.
9. Hall B, Andreeff M, Marini F. The participation of mesenchymal stem cells in tumor stroma formation and their application as targeted-gene delivery vehicles. *Handb Exp Pharmacol* 2007; 263–283.
10. Le Blanc K, Ringden O. Immunobiology of human mesenchymal stem cells and future use in hematopoietic stem cell transplantation. *Biol Blood Marrow Transplant* 2005; **11**: 321–334.
11. Studeny M, Marini FC, Champlin RE, *et al.* Bone marrow-derived mesenchymal stem cells as vehicles for interferon-beta delivery into tumors. *Cancer Res* 2002; **62**: 3603–3608.
12. Okada T, Caplen NJ, Ramsey WJ, *et al.* In situ generation of pseudotyped retroviral progeny by adenovirus-mediated transduction of tumor cells enhances the killing effect of HSV-tk suicide gene therapy in vitro and in vivo. *J Gene Med* 2004; **6**: 288–299.
13. Nakamura K, Ito Y, Kawano Y, *et al.* Antitumor effect of genetically engineered mesenchymal stem cells in a rat glioma model. *Gene Ther* 2004; **11**: 1155–1164.
14. Aluigi M, Fogli M, Curti A, *et al.* Nucleofection is an efficient nonviral transfection technique for human bone marrow-derived mesenchymal stem cells. *Stem Cells* 2006; **24**: 454–461.
15. Aggarwal S, Pittenger MF. Human mesenchymal stem cells modulate allogeneic immune cell responses. *Blood* 2005; **105**: 1815–1822.
16. Le Blanc K, Rasmusson I, Sundberg B, *et al.* Treatment of severe acute graft-versus-host disease with third party haploidentical mesenchymal stem cells. *Lancet* 2004; **363**: 1439–1441.
17. Barry FP, Murphy JM, English K, *et al.* Immunogenicity of adult mesenchymal stem cells: lessons from the fetal allograft. *Stem Cells Dev* 2005; **14**: 252–265.

THE JOURNAL OF BIOLOGICAL CHEMISTRY VOL. 284, NO. 6, pp. 3379–3388, February 6, 2009

The Factor VIIIa C2 Domain (Residues 2228–2240) Interacts with the Factor IXa Gla Domain in the Factor Xase Complex*

Received for publication, June 30, 2008, and in revised form, October 30, 2008 Published, JBC Papers in Press, December 1, 2008, DOI 10.1074/jbc.M804955200

Tetsuhiro Soeda[‡], Keiji Nogami[‡], Katsumi Nishiya[‡], Masahiro Takeyama[‡], Kenichi Ogiwara[‡], Yoichi Sakata[§], Akira Yoshioka[‡], and Midori Shima[‡1]

From the [‡]Department of Pediatrics, Nara Medical University, Kashihara, Nara 634-8522, Japan and the [§]Division of Cell and Molecular Medicine, Center for Molecular Medicine, Jichi Medical University, Tochigi-ken 329-0498, Japan

Factor VIIIa functions as a cofactor for factor IXa in the phospholipid surface-dependent activation of factor X. Both the C2 domain of factor VIIIa and the Gla domain of factor IXa are involved in phospholipid binding and are required for the activation of factor X. In this study, we have examined the close relationship between these domains in the factor Xase complex. Enzyme-linked immunosorbent assay-based and surface plasmon resonance-based assays in the absence of phospholipid showed that Glu-Gly-Arg active site-modified factor IXa bound to immobilized recombinant C2 domain (rC2) dose-dependently (K_d = 108 nM). This binding ability was optimal under physiological conditions. A monoclonal antibody against the Gla domain of factor IXa inhibited binding by ~95%, and Gla domainless factor IXa failed to bind to rC2. The addition of monoclonal antibody or rC2 with factor VIIIa inhibited factor IXa-catalyzed factor X activation in the absence of phospholipid. Inhibition was not evident, however, in similar experiments in the absence of factor VIIIa, indicating that the C2 domain interacted with the Gla domain of factor IXa. A fragment designated C2-(2182–2259), derived from V8 protease-cleaved rC2, bound to Glu-Gly-Arg active site-modified factor IXa. Competitive assays, using overlapping synthetic peptides encompassing residues 2182–2259, demonstrated that peptide 2228–2240 significantly inhibited both this binding and factor Xa generation, independently of phospholipid. Our results indicated that residues 2228–2240 in the factor VIIIa C2 domain constitutes an interactive site for the Gla domain of factor IXa. The findings provide the first evidence for an essential role for this interaction in factor Xase assembly.

Factor VIII, a plasma protein that participates in the blood coagulation cascade, is deficient or defective in individuals with hemophilia A. Factor VIII circulates in plasma as a noncovalent complex with VWF,[2] which stabilizes the synthesis and activity of the cofactor. Mature factor VIII is synthesized as a single chain polypeptide of ~300 kDa consisting of 2,332 amino acid residues (1, 2). Based on internal homologies of the amino acid sequence, factor VIII has three types of domains arranged in the order of A1-A2-B-A3-C1-C2 (3). Factor VIII circulates in the plasma as a heterodimer of a heavy chain, consisting of the A1, A2, and heterogeneous fragments of partially proteolyzed B domains, together with a light chain consisting of the A3, C1, and C2 domains (1, 3).

The carboxyl-terminal 159 amino acids of factor VIII comprise the C2 domain, which is involved in binding to both VWF (4–6) and phospholipid membrane surfaces (6, 7). Binding in this domain appears to be competitive and mutually exclusive (4, 5, 8, 9). The C2 domain has also been shown to participate in binding to factor Xa and thrombin (10, 11). Additionally, a major epitope for allo- and autoantibodies and for monoclonal antibodies has been located within the C2 domain (4, 6, 12), indicating that this region could be an antigenic "hot spot." Consequently, important aspects of the expression and regulation of factor VIII appear to be governed by the structure and function of the C2 domain.

Factor VIIIa functions as a cofactor for factor IXa in the anionic, phospholipid surface-dependent conversion of factor X to Xa. In intrinsic factor Xase, factor VIIIa binds to factor IXa and increases the k_{cat} for factor Xa formation by several orders of magnitude compared with factor IXa alone (13). The A2 domain of factor VIIIa interacts with the catalytic domain of factor IXa, and the A3 domain interacts with the first epidermal growth factor domain (14). Although the affinity of isolated A2 for factor IXa is low (K_d ~ 300 nM), it amplifies the enzyme activity of factor IXa by modulating an active site in the catalytic domain, and this interaction defines the cofactor activity of factor VIIIa (15). Factor IXa-interactive sites in the A2 domain are located in at least three regions, within residues 484–509 (16), 558–565 (17), and 708–717 (18), respectively.

In contrast, the high affinity (K_d ~ 15 nM) of the isolated factor VIIIa light chain for factor IXa provides the majority of the binding energy for this interaction. To date, one region within the A3 domain, residues 1804–1818, has been identified

* This work was supported in part by MEXT KAKENHI Grant 19591264 and the Mitsubishi Pharma Research Foundation. A preliminary account of this work was presented at the 49th Annual Meeting of the American Society of Hematology, December 9, 2007, Atlanta, GA. The costs of publication of this article were defrayed in part by the payment of page charges. This article must therefore be hereby marked "*advertisement*" in accordance with 18 U.S.C. Section 1734 solely to indicate this fact.

[1] To whom correspondence should be addressed: Dept. of Pediatrics, Nara Medical University, 840 Shijo-cho, Kashihara, Nara 634-8522, Japan. Tel.: 81-744-29-8881; Fax: 81-744-24-9222; E-mail: roc-noga@naramed-u.ac.jp.

[2] The abbreviations used are: VWF, von Willebrand factor; Gla, γ-carboxyglutamic acid; rC2, recombinant C2 domain; HRP, horseradish peroxidase; GDless, Gla domainless; EGR-ck, Glu-Gly-Arg-chloromethylketone; HPLC, high performance liquid chromatography; LC/MS, liquid chromatography coupled to mass spectrometry; EGR-factor IXa, Glu-Gly-Arg active site-modified factor IXa; EGR-GDless factor IXa, Glu-Gly-Arg active site-modified Gla domainless factor IXa; BSA, bovine serum albumin; SPR, surface plasmon resonance; ELISA, enzyme-linked immunosorbent assay; mAb, monoclonal antibody.

as a factor IXa-interactive site (19, 20). Recently, Blostein *et al.* (21) demonstrated that the light chain of factor VIIIa interacts with the Gla domain of factor IXa, which contains 12 post-translationally modified glutamic acid residues (γ-carboxyglutamic acid) and functions in calcium-dependent phospholipid binding (22). However, the site in the light chain of factor VIIIa responsible for interaction with the Gla domain of factor IXa remains to be identified. The C2 domain of factor VIIIa and the Gla domain of factor IXa are involved in phospholipid binding, and both bound sequences could be aligned structurally close. We speculated, therefore, that the C2 domain of factor VIIIa might interact with the Gla domain of factor IXa in the factor Xase complex.

In the present study, we have examined the interaction between the C2 domain of factor VIIIa and the Gla domain of factor IXa in the factor Xase complex, using a combination of functional and binding assays employing recombinant C2 domain (rC2), V8 protease-digested C2 fragments, synthetic peptides, and monoclonal antibodies. Our results indicated that residues 2228–2240 in the C2 domain contain an interactive site for the Gla domain of factor IXa. The findings provide the first evidence for an essential role of this interaction in factor Xase assembly.

MATERIALS AND METHODS

Reagents—Purified recombinant factor VIII was a generous gift from Bayer Corp. (Osaka, Japan). Two monoclonal antibodies, mAb IXa-GD, against the Gla domain of factor IXa and specific for calcium-dependent conformation, and mAb 3A6 against the heavy chain of factor IXa, were prepared (23, 24). A monoclonal antibody, ESH8, against the C2 domain of factor VIII and recognizing residues 2248–2285 (4, 5) was purchased from American Diagnostica Inc. (Stamford, CT). A horseradish peroxidase (HRP)-labeled monoclonal antibody was prepared using Peroxidase Labeling Kit-NH_2 (Dojindo Molecular Technologies Inc., Kumamoto, Japan). Human factor IXa, factor X, and EGR-ck (Hematologic Technologies, Inc., Essex Junction, VT), factor Xa (Enzyme Research Laboratories, Inc., South Bend, IN), thrombin (Sigma), recombinant hirudin (Calbiochem), and chromogenic Xa substrate S-2222 (Chromogenix, Milano, Italy) were purchased commercially. Gla domainless (GDless) factor IXa was prepared from factor IXa by limited chymotryptic digestion (25). Briefly, α-chymotrypsin was incubated with factor IXa in a 1:24 ratio (w/w) at 4 °C. The reaction was then quenched using 5 mM diisopropyl fluorophosphate, and the GDless factor IXa was separated from undigested factor IXa and the Gla domain-containing peptide (residues 1–42) using ion exchange chromatography. Molecular mass was estimated by SDS-PAGE. The amidolytic activity of GDless factor IXa was less than 0.2%. Phospholipid vesicles containing 10% phosphatidylserine, 60% phosphatidylcholine, and 30% phosphatidylethanolamine (Sigma) were prepared using *N*-octyl glucoside (26). Synthetic peptides consisting of overlapping sequences of 13 residues encompassing 2182–2249 within the factor VIII C2 domain were prepared by Biosynthesis (Lewisville, TX). They were purified by reverse phase HPLC (purity >95%) and were confirmed by mass spectrometry analysis.

Construction, Expression, and Purification of Factor VIII rC2—The rC2 was prepared using the protocol described by Takeshima *et al.* (27). Briefly, cDNA encoding the C2 domain of human factor VIII with a 4-amino acid NH_2-terminal extension (Val^{2169}–Tyr^{2332}) was constructed, transformed, and expressed in *Pichia pastoris* cells. The product was purified using ammonium sulfate fractionation and cation exchange HPLC (TSK-GEL CM-3SW; TOSOH Corp., Tokyo, Japan). SDS-PAGE analysis demonstrated >95% purity. The rC2 protein was identified as a single peak by a gel filtration and had a mass 18,626.6 on LC/MS analysis, closely matching the expected mass of 18,627.3.

Preparation of EGR-GDless Factor IXa—Factor IXa (10 μM) or GDless factor IXa (2.3 μM) was inactivated overnight at 4 °C by the addition of a 20-fold molar excess of EGR-ck in 20 mM HEPES, pH 7.2, 150 mM NaCl, and 0.01% Tween 20 (HBS buffer). Unbound EGR-ck was removed by extensive dialysis at 4 °C in the same buffer. Chromogenic assays demonstrated less than 0.2% residual activity of factor IXa or GDless factor IXa, respectively.

Preparation of rC2 Proteolytic Fragments—The rC2 (16.7 μM) was digested for 96 h at 37 °C with *Staphylococcus aureus* V8 protease (5.4 μM; Wako Pure Chemical Industries Ltd., Osaka, Japan) in 100 mM Tris-Tricine, pH 8.4, 150 mM NaCl, and 0.1% SDS. The digest was treated with the SDS-Out™ precipitation kit (Pierce) to remove the SDS and was fractionated by reverse phase HPLC using TSKgel ODS-100Z (5 μm; Tosoh Corp.). The reaction mixture was loaded onto a column equilibrated with 90% distilled H_2O, 10% acetonitrile in 0.1% trifluoroacetic acid and eluted with a linear gradient of 10–50% acetonitrile over 60 min. Fragments were detected at 216 nm and automatically collected in 500-μl aliquots and lyophilized. The fragments exhibited excellent solubility following their resuspension in HBS buffer. Protein concentrations were determined by the method of Bradford (28). Electrophoresis of the purified fragments followed by staining with GelCode Blue Stain Reagent (Pierce) showed >95% purity.

ELISA-based Binding Assay—Microtiter wells were coated with 200 nM rC2 (100 μl) in 100 mM sodium bicarbonate, pH 9.6, overnight at 4 °C. The wells were washed with HBS buffer and were blocked with the same buffer containing 5% BSA for 2 h at 37 °C. EGR-factor IXa or EGR-GDless factor IXa was then added and incubated in HBS buffer containing 1 mM $CaCl_2$ and 5% BSA for 2 h at 37 °C. Bound EGR-factor IXa was quantified by the addition of HRP-labeled anti-factor IXa mAb 3A6 and *o*-phenylenediamine dihydrochloride substrate. Reactions were quenched by the addition of 2 M H_2SO_4, and absorbances were measured at 492 nm using a Labsystems Multiskan Multisoft microplate reader (Labsystems, Helsinki, Finland). Control experiments demonstrated that mAb 3A6 did not affect the reaction between factor VIII and factor IXa (data not shown). The amount of nonspecific binding of HRP-labeled IgG in the absence of factor VIII was <5% of the total signal. Specific binding was recorded after subtracting the nonspecific binding. In competitive inhibition assays, the competitor proteins were incubated with 100 nM EGR-factor IXa for 2 h at 37 °C prior to the addition to immobilized rC2. The percentage of inhibition was calculated using the equation, (bound absorbance − non-

specific absorbance)/(maximum − nonspecific) × 100 (%). Absorbance in the absence of competitive protein or immobilized rC2 was regarded as maximum or nonspecific, respectively.

SPR-based Binding Assay—The kinetics of rC2 and EGR-factor IXa interaction were determined in SPR-based assays using a Biacore X instrument (BIAcore AB, Uppsala, Sweden). EGR-factor IXa was covalently coupled to the surface of a CM5 chip at a coupling density of ~7 ng/mm^2. Binding (association) of the ligand was monitored in 10 mM HEPES, pH 7.4, 150 mM NaCl, 1 mM $CaCl_2$, and 0.005% surfactant P20, at a flow rate of 20 μl/min for 2 min at 37 °C. The dissociation of bound ligand was monitored for a 2-min period by replacing the ligand-containing buffer with buffer alone. The level of nonspecific binding corresponding to ligand binding to the uncoated chip was subtracted from the signal. The rate constants for association (k_a) and dissociation (k_d) were determined by nonlinear regression analysis (29, 30) using the evaluation software provided by Biacore AB. Equilibrium dissociation constants (K_d) were calculated as k_d/k_a.

Factor Xa Generation Assays—The rate of conversion of factor X to factor Xa was monitored in a purified system (18, 31). Factor Xa was generated at 22 °C in HBS buffer containing 1 mM $CaCl_2$ and 0.1% BSA. For assays in the absence of phospholipid, 200 nM factor VIII was activated by 10 nM thrombin. Thrombin activity was inhibited after 1 min by the addition of 2.5 units/ml hirudin, and factor Xa generation was initiated by the addition of 5 nM factor IXa and 1 μM factor X. Experiments in the absence of factor VIIIa were performed under the same conditions except for 20 nM factor IXa. For assays in the presence of phospholipid, 30 nM factor VIII was activated by 10 nM thrombin in the presence of 20 μM phospholipid. Thrombin activity was inhibited after 1 min by hirudin, and factor Xa generation was initiated by the addition of 0.5 nM factor IXa and the indicated amounts of factor X. Aliquots were removed at appropriate times to assess initial rates of product formation and added to tubes containing EDTA (100 mM final concentration) to stop the reaction. Rates of factor Xa generation were determined at 405 nm using a microtiter plate reader after the addition of chromogenic substrate, S-2222 (0.46 mM final concentration). Factor Xa generation was quantified by extrapolation from a standard curve prepared using known amounts of factor Xa.

ELISA for Factor VIII or EGR-factor IXa Binding to Phosphatidylserine—ELISA were performed using a minor modification of a previously reported method (7). Briefly, 50 μM 1,2-dioleoyl-*sn*-glycero-3-phospho-L-serine (Sigma) in methanol was immobilized onto each well of a microtiter plate and allowed to air dry at 4 °C overnight. After washing with HBS buffer, the wells were blocked for 2 h at 37 °C with HBS buffer containing 5% BSA. Factor VIII or EGR-factor IXa was added to each well in HBS buffer containing 1 mM $CaCl_2$ and 5% BSA and incubated for 2 h at 37 °C. Bound factor VIII was detected using anti-factor VIII mAb ESH8, followed by HRP-labeled anti-mouse second antibody. Bound EGR-factor IXa was detected using HRP-labeled mAb 3A6.

NH_2-terminal Sequence Analysis—The C2 fragments were blotted onto polyvinylidene difluoride membranes, stained with Gelcode Blue, and excised. NH_2-terminal sequence analyses of the purified fragments were performed using an Applied Biosystems model 491 sequencer (Foster City, CA). Samples were subjected to 5 or 7 cycles of automated sequencing.

Solvent-accessible Surface Area Analysis—The solvent accessibilities at the interface for the residues 2182–2259 of the C2 domain were calculated from the atomic coordinates using Marc Gerstein's calc-surface program (32) available from the Helix Systems Web site. The atomic coordinates of human factor VIII and C2 domain were retrieved from the Protein Data Bank (code 2R7E and 1D7P, respectively). Values that are more positive represent a greater probability of surface exposure.

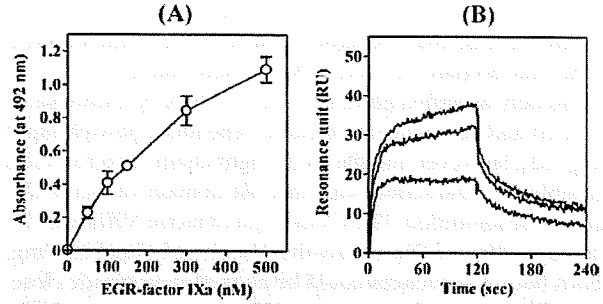

FIGURE 1. **Direct binding of EGR-factor IXa to rC2.** *A*, ELISA-based assay. Various concentrations of EGR-factor IXa were reacted with rC2 (200 nM) that had been immobilized onto microtiter wells for 2 h at 37 °C, as described under "Materials and Methods." Bound EGR-factor IXa was detected using HRP-labeled anti-factor IXa mAb 3A6. Absorbance values were plotted as a function of the concentration of EGR-factor IXa. Experiments were performed at least three separate times, and average ± S.D. values are shown. *B*, SPR-based assay. Various concentrations of rC2 were injected onto the EGR-factor IXa (~7 ng/mm^2) immobilized onto the sensor chip at a flow rate of 20 μl/min for 2 min, followed by a change of running buffer for 2 min as described under "Materials and Methods." The *three lines* illustrate representative response curves for the different concentrations of rC2 (100, 300, and 500 nM, respectively). Experiments were performed at least three separate times.

RESULTS

Binding of EGR-factor IXa to the C2 Domain—Blostein *et al.* (21) have recently reported that the Gla domain of factor IXa interacts with the light chain of factor VIIIa. The C2 domain of factor VIIIa and the Gla domain of factor IXa are involved in phospholipid-binding, and we surmised, therefore, that they could be juxtaposed in the factor Xase complex and that the C2 domain might associate directly with the Gla domain of factor IXa. To investigate this hypothesis, we initially examined the direct binding of factor IXa to immobilized rC2 using microtiter-based, solid phase binding assays. An active site-modified EGR-factor IXa preparation was used in these experiments to eliminate difficulties of interpretation in the presence of enzymatically active factor IXa. Various concentrations of EGR-factor IXa were incubated with immobilized rC2 (200 nM). Bound EGR-factor IXa was detected using anti-factor IXa mAb 3A6, recognizing the heavy chain of its protease. EGR-factor IXa bound to immobilized rC2 in a dose-dependent manner (Fig. 1*A*). Control experiments using an anti-C2 mAb demonstrated that immobilized rC2 was not affected by the ionic strength of the wash buffer or the duration of the wash and incubation steps subsequent to C2 binding (data not shown). To confirm the specificity of this binding, various concentrations of factor VIII or rC2 were preincubated with EGR-factor IXa (100 nM) in

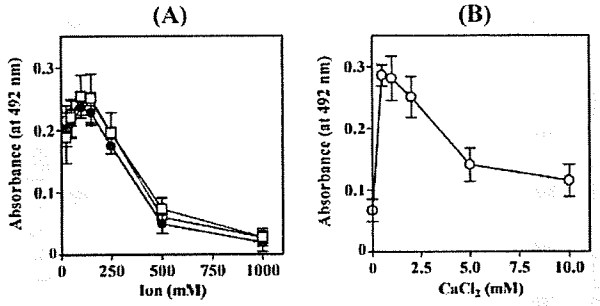

FIGURE 2. **Effect of ionic strength on EGR-factor IXa and rC2 interaction.** *A*, NaCl, KCl, and LiCl effect. EGR-factor IXa (100 nM) was incubated with immobilized rC2 (200 nM) in HBS buffer containing 1 mM $CaCl_2$, 5% BSA, and various amounts of NaCl (*open circles*), KCl (*closed circles*), and LiCl (*open squares*) in an ELISA-based assay. *B*, $CaCl_2$ effect. EGR-factor IXa was incubated with immobilized rC2 in HBS buffer containing 5% BSA and various amounts of $CaCl_2$. EGR-factor IXa bound in the absence of $CaCl_2$ refers to an experiment in the presence of 10 mM EDTA. Experiments were performed at least three separate times, and average ± S.D. values are shown.

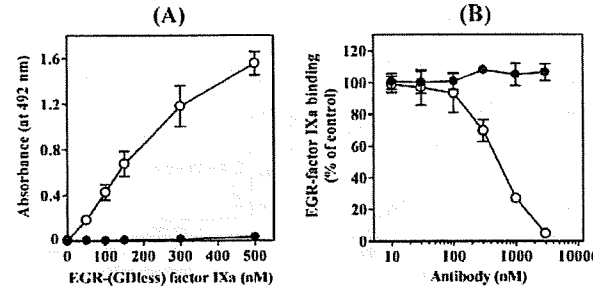

FIGURE 3. **Contribution of the Gla domain of EGR-factor IXa for rC2 interaction.** *A*, various concentrations of EGR-factor IXa (*open circles*) or EGR-GDless factor IXa (*closed circles*) were incubated with immobilized rC2 (200 nM) for 2 h at 37 °C in an ELISA-based assay. *B*, EGR-factor IXa (100 nM) was preincubated with various concentrations of mAb IXa-GD IgG (*open circles*) or normal murine IgG (*closed circles*) for 2 h at 37 °C, prior to incubation with immobilized rC2. Absorbance values for the EGR-factor IXa binding to rC2 in the absence of competitor represent the 100% level. The percentage of EGR-factor IXa binding was plotted as a function of antibody concentration. Experiments were performed at least three separate times, and average ± S.D. values are shown.

the fluid phase prior to addition to the immobilized rC2. Factor VIII and rC2 inhibited EGR-factor IXa binding to immobilized rC2 by ~90 and ~60%, respectively (data not shown), confirming specificity of the assay.

We further evaluated interactions by an alternative approach using real time SPR-based assays. This technique provides information on kinetic and equilibrium binding constants (29, 30). A range of concentrations of rC2 were added to EGR-factor IXa immobilized onto a sensor chip. Fig. 1*B* shows representative curves corresponding to the association/dissociation of rC2. The data could be comparatively well fitted by nonlinear regression using a 1:1 binding model with drifting base line. Kinetic constants showed that rC2 bound to EGR-factor IXa with mild affinity (K_d = 108 ± 27 nM, $k_d/k_a = 2.45 \times 10^{-2}$ $s^{-1}/2.36 \times 10^5$ M^{-1} s^{-1}). In ELISA-based assays, the apparent K_d value appeared to be higher (~400 nM), compared with that obtained by SPR-based assays. Since ELISA is not an equilibrium binding assay, the multiple steps of incubation and wash may affect the detection for lower concentrations of EGR-FIXa. The results indicated that the C2 domain of factor VIII interacted directly with factor IXa.

Characterization of the Interaction between the C2 Domain and EGR-factor IXa—The light chain of factor VIIIa interacts with factor IXa in electrostatic and calcium-dependent mechanisms (19). To further characterize this interaction, factor IXa (100 nM) was mixed with various amounts of NaCl and incubated with immobilized rC2. Control experiments showed that the amount of immobilized rC2 or the reactivity of antibody was not affected even at a higher concentration of NaCl (data not shown). Binding of EGR-factor IXa to rC2 was maximal at physiological concentrations of NaCl (~150 mM; Fig. 2*A*). Higher concentrations of NaCl incrementally weakened this interaction, however, and consequently binding was significantly decreased by ~95% at elevated ionic strengths, supporting the salt sensitivity of this interaction. The Na^+-bound factor IXa drastically enhances catalytic activity toward factor X and increases the affinity for factor VIIIa (33, 34). However, other monovalent cations, K^+ and Li^+, also inhibited this binding similarly, suggesting that this effect was not due to a specific interaction of Na^+-factor IXa.

Ca^{2+} is known to be required for the structural and functional integrity of factor IXa, and hence the effect of Ca^{2+} on factor IXa-rC2 interaction was also examined in the current experiments. Binding of factor IXa to immobilized rC2 was investigated in buffer containing various amounts of $CaCl_2$. EDTA (10 mM) was added to the reaction mixtures to assess binding in the absence of Ca^{2+}. The presence of Ca^{2+} up to ~1.0 mM markedly increased factor IXa binding by ~6-fold compared with that in the absence of Ca^{2+} (Fig. 2*B*). Optimal binding was observed at approximately physiological concentrations of free Ca^{2+} (~1.3 mM). Binding was significantly inhibited by increments of Ca^{2+} >1 mM. The data were consistent, therefore, with a role for Ca^{2+} in C2-factor IXa interaction, although it was not possible to distinguish between a direct or indirect role for Ca^{2+} in mediating this effect.

Binding of the Gla Domain of Factor IXa to the C2 Domain—To investigate whether the Gla domain of factor IXa participates in direct interactions with the C2 domain of factor VIII, EGR-GDless factor IXa was prepared by chymotrypsin digestion and EGR-ck labeling, as described under "Materials and Methods." Control experiments demonstrated that EGR-GDless factor IXa and EGR-factor IXa were similarly reactive with anti-factor IXa mAb 3A6 in the ELISA (data not shown). The binding of EGR-GDless factor IXa to immobilized rC2 was markedly lower than that of EGR-factor IXa even at the maximum concentration employed (500 nM; Fig. 3*A*). SPR-based assays also showed that rC2 failed to react with EGR-GDless factor IXa (data not shown). In addition, competitive experiments using an anti-factor IXa mAb, mAb IXa-GD, recognizing the Gla domain of factor IXa and dependent on the presence of Ca^{2+}, demonstrated that the monoclonal antibody blocked binding of EGR-factor IXa to rC2 (up to ~95%) in a dose-dependent manner (IC_{50}; 758 ± 93 nM) (Fig. 3*B*). These findings were in keeping with a significant role for the Gla domain of factor IXa in direct binding to the C2 domain of factor VIII.

To assess the functional role of the interaction between the C2 domain and Gla domain of factor IXa in the factor Xase complex, we examined the effect of rC2 or mAb IXa-GD on factor VIIIa/factor IXa-mediated activation of factor X in an

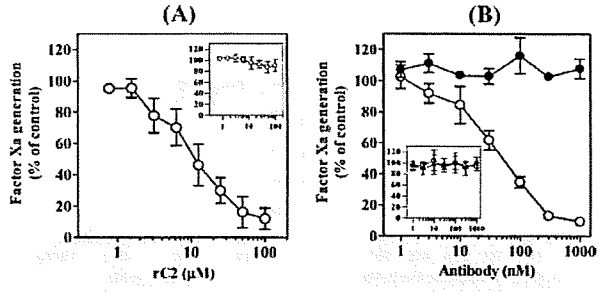

FIGURE 4. **Inhibition of rC2 and mAb IXa-GD in factor VIIIa/factor IXa-mediated factor X activation in the absence of phospholipid.** Various concentrations of rC2 (*open circles*) (*A*) or mAb IXa-GD (*open circles*) (*B*) or normal murine IgG (*closed circles*) were preincubated with 5 nM factor IXa for 2 h at 37 °C. Factor Xa generation was initiated by the addition of thrombin-activated factor VIIIa (200 nM) and 1 μM factor X under the conditions described under "Materials and Methods." The initial rate of factor Xa generated in the absence of competitor represents the 100% level and was 1.19 ± 0.14 nM/min. Initial rates of factor Xa generation were plotted as a function of rC2 or antibody concentration. The *inset* shows the experiments in the absence of factor VIIIa under similar conditions except for 20 nM factor IXa. The initial rate of factor Xa generated in the absence of competitor (100% level) was 0.0034 ± 0.0001 nM/min. Experiments were performed at least three separate times, and average ± S.D. values are shown.

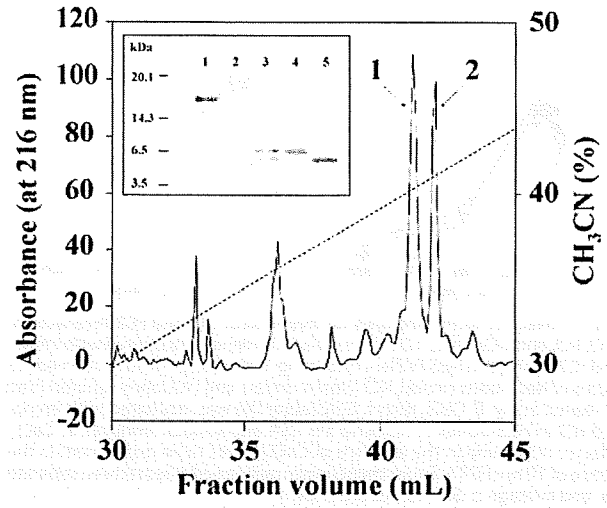

FIGURE 5. **Reverse phase HPLC and SDS-PAGE of V8 protease-cleaved rC2.** *S. aureus* V8 protease-cleaved C2 fragments were fractionated by reverse phase HPLC. The *broken line* represents acetonitrile concentration (10–50%), and fragments were detected at 216 nm (*solid line*). The *inset* shows that the proteins were analyzed by SDS-PAGE using 16.5% peptide gel under nonreducing conditions, followed by staining with GelCode Blue. *Lane 1*, 1.5 μg of rC2; *lane 2*, 0.75 μg of V8 protease; *lane 3*, 1.5 μg of rC2 digested with 0.75 μg of V8 protease; *lane 4*, 0.5 μg of fragment in peak fraction 1; *lane 5*, 0.5 μg of fragment in peak fraction 2. The positions of molecular mass markers in kDa are indicated to the *left*.

amidolytic assay. For this assay, 200 nM factor VIII was activated by thrombin and incubated with mixtures of 5 nM factor IXa and various concentrations of rC2 or mAb IXa-GD. Factor Xa generation was initiated by the addition of 1 μM factor X. The rC2 competes with factor VIII for binding to phospholipid membranes, and for this reason, the assays were performed in the absence of phospholipid. The addition of rC2 and mAb IXa-GD markedly decreased the rates of factor Xa generation (by >90%) in a dose-dependent manner, with the IC_{50} values of 10.9 ± 3.8 μM and 43.2 ± 15.3 nM, respectively (Fig. 4, *A* and *B*). To exclude the possibility that rC2 and mAb IXa-GD directly affected factor IXa-catalyzed activation of factor X, factor Xa generation was further examined in the absence of factor VIIIa. As expected, there was little inhibition of factor Xa generation in the presence of rC2 or mAb IXa-GD (Fig. 4, *inset*), confirming that the reactions were governed by factor VIIIa. The results indicated that association between the C2 domain of factor VIII and the Gla domain of factor IXa played a significant role in the assembly of the factor Xase complex and hence factor IXa-catalyzed activation of factor X in the presence of factor VIIIa.

Purification and Characterization of rC2-digested Fragments—To localize factor IXa-interactive regions within the C2 domain, limited *Staphylococcus aureus* V8 protease digests of rC2 were prepared. SDS-PAGE analysis demonstrated the presence of two large fragments of apparent mass 7.5- and 6.2-kDa that were significantly smaller than the initial rC2 (~16 kDa) (Fig. 5*B*). The digestion of rC2 by V8 protease required denaturing conditions with 0.1% SDS, and we confirmed that the binding of SDS-treated, uncleaved rC2 to EGR-factor IXa was similar to that of the non-SDS-treated product in the ELISA-based assay (data not shown). EGR-factor IXa bound to immobilized, unfractionated V8 protease-cleaved rC2 in a dose-dependent manner (data not shown), prompting us to further isolate and purify the cleaved fragments. The two fragments were not able to be separated by ion exchange HPLC using CM, Mono-Q, and Mono-S under any salt and pH conditions but were resolved by reverse phase HPLC (Fig. 5). SDS-PAGE confirmed that these fractions, designated as peak 1 and peak 2, represented the 7.5- and 6.2-kDa fragments, respectively (Fig. 5, *inset*). Some smaller peaks were observed, but the bands were poorly detectable in SDS-PAGE and appeared to represent further minor degradation of rC2. The peak 1 and peak 2 fractions were further characterized by size exclusion chromatography, and each was shown to elute as a single peak, indicating that the fragments were monomeric in solution (data not shown).

Automated NH_2-terminal sequence analysis identified that the sites of cleavage responsible for the generation of the two C2 fragments were located at residues Glu^{2181}-Ser^{2182} and Glu^{2259}-Phe^{2260} for the ~7.5- and ~6.2-kDa fragments, respectively (Table 1). In addition, LC/MS analysis indicated that the molecular mass of fragment 1 (7.5 kDa) and fragment 2 (6.2 kDa) was 8827.25 ± 5.70 and 7355.63 ± 0.68 Da, respectively. On the basis of the previous molecular masses determined by LC/MS, NH_2-terminal sequence analysis, and specificity of V8 protease cleavage site (-Glu-*X* and/or -Asp-*X*), the deduced protein sequences of the two C2 fragments matched Ser^{2182}–Glu^{2259} (expected mass, 8823.08 Da) and Phe^{2260}–Glu^{2322} (expected mass, 7354.39 Da). Hence, the ~7.5- and ~6.2-kDa C2 fragments were designated as C2-(2182–2259) and C2-(2260–2322), respectively.

Binding of the Isolated C2 Fragments to EGR-factor IXa and the Effects on Factor Xa Generation—To determine whether the C2-(2182–2259) and/or C2-(2260–2322) were able to bind to factor IXa, we investigated direct binding in ELISA-based assays, as described above. EGR-factor IXa bound directly to immobilized C2-(2182–2259) (600 nM) in a dose-dependent manner, although in this instance, the binding efficiency was weaker than that of the uncleaved rC2 (Fig. 6*A*). In contrast, very limited binding of EGR-factor IXa to immobilized

TABLE 1

Amino-terminal sequence analysis of the C2 fragments

Sequences were determined as described under "Materials and Methods" and were aligned using published factor VIII sequences (1, 2).

	Cycle number						
	1	2	3	4	5	6	7
Residues 2182–2188	Ser	Lys	Ala	Ile	Ser	Asp	Ala
C2 fragment 1	Ser	Lys	Ala	Ile	Ser	Asp	Ala
pmol	10.4	17.7	14.4	14.3	8.4	6.6	7.9
Residues 2260–2264	Phe	Leu	Ile	Ser	Ser		
C2 fragment 2	Phe	Leu	Ile	Ser	Ser		
pmol	10.7	10.3	11.0	5.5	5.4		

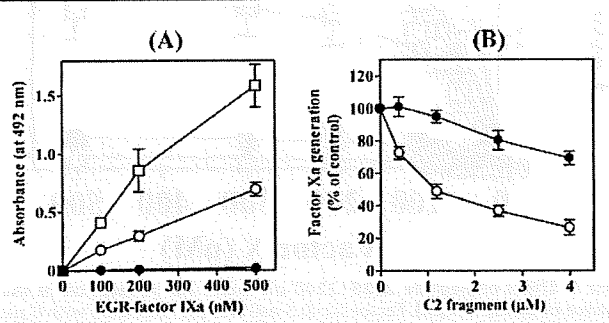

FIGURE 6. **Binding of EGR-factor IXa to C2 fragments and the inhibitory effects on factor Xa generation.** A, binding of EGR-factor IXa. Various concentrations of EGR-factor IXa were incubated with immobilized C2-(2182–2259) (600 nM; *open circles*), C2-(2260–2322) (600 nM; *closed circles*), and intact rC2 (100 nM; *open squares*) for 2 h at 37 °C in an ELISA-based assay. Absorbance values were plotted as a function of the concentration of EGR-factor IXa. *B*, inhibition of factor Xa generation in the absence of phospholipid. Various amounts of C2-(2182–2259) (*open circles*) or C2-(2260–2322) (*closed circles*) were preincubated with 5 nM factor IXa for 2 h at 37 °C, and factor Xa generation was initiated with the addition of thrombin-activated factor VIIIa (200 nM) and 1 μM factor X. The initial rate of factor Xa generated in the absence of competitor (100% level) was 1.46 ± 0.19 nM/min. Initial rates of factor Xa generation were plotted as a function of C2 fragment concentration. Experiments were performed at least three separate times, and average ± S.D. values are shown.

C2-(2260–2322) was observed. In control experiments, EGR-GDless factor IXa did not bind to either immobilized C2 fragment (data not shown). To assess the functional capacity of the two C2 fragments in factor Xase assembly, amidolytic assays were again repeated in the absence of phospholipid. Factor VIII (200 nM) was activated by thrombin and incubated with factor IXa (5 nM)/C2 fragment mixtures and factor X (1 μM). The C2-(2182–2259) competitively inhibited factor Xa generation by ~80% at the maximum concentration employed (IC_{50} = 1.2 μM; Fig. 6*B*). The effect of C2-(2260–2322) was significantly lower than that of C2-(2182–2259), however, and inhibited factor Xa generation by ~30%. Collectively, these data suggest that an interactive site(s) for the Gla domain of factor IXa was likely to be located within residues 2182–2259 of the C2 domain.

Effects of Synthetic C2 Peptides on rC2 and EGR-factor IXa Interaction and on Factor Xa Generation in the Absence of Phospholipids—On the basis of the competitive binding assays and ELISA, we focused on the 2182–2259 region in the C2 domain to further identify the potential factor IXa-interactive site. The C2-factor IXa interaction is electrostatically dependent (see Fig. 2*A*), suggesting that both interactive sites are surface-exposed. The analysis of solvent-accessible surface area was utilized, therefore, to examine regions within residues 2182–2259 exhibiting a high probability of being surface-exposed. The solvent accessibilities at the interface were calcu-

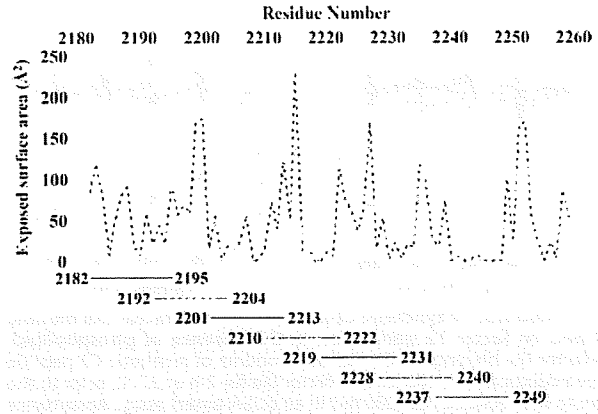

FIGURE 7. **Accessible surface area of residues 2182–2259 of the C2 domain.** The solvent accessibilities at the interface for the residues 2182–2259 of the C2 domain were calculated from the atomic coordinates in the structure of factor VIII (*solid lines*) and C2 (*dashed lines*) using Marc Gerstein's calc-surface program (see "Materials and Methods"). Accessible surface area (Å²) was used to estimate the probability of a segment being exposed to the surface. Synthetic peptides corresponding to regions of high surface probability are indicated by the *horizontal bars* and are identified by residue numbers for the segments.

lated from atomic coordinates in the structures of factor VIII and C2 (Protein Data Bank code 2R7E and 1D7P, respectively), and they were similar. Using this approach, overlapping synthetic peptides encompassing the 2182–2249 region were prepared (Fig. 7). Since the C2-factor IXa interaction was not affected by anti-C2 mAb ESH8 with epitopes 2248–2285 (data not shown), the 2248–2259 region was excluded. Effects of peptides to block C2-factor IXa interaction and to inhibit factor Xa generation were examined.

The synthetic peptide corresponding to residues 2228–2240 (designated peptide 2228–2240) inhibited binding of EGR-factor IXa to rC2 by ~75% at the maximum concentrations employed (at 1 mM) (Fig. 8*A*). The IC_{50} value was ~400 μM. The other six peptides, corresponding to residues 2182–2195, 2192–2204, 2201–2213, 2210–2222, 2219–2231, and 2237–2249, demonstrated no inhibitory effects. Moreover, a control peptide (VKMTKQFDVQLWE), comprising the 2228–2240 residues in a random sequence, completely lost the ability to inhibit this interaction (data not shown). The inhibitory effects of these peptides were further studied in the factor Xa generation assay. The peptide 2228–2240, which blocked C2-factor IXa interaction, depressed factor Xa generation by ~75% at the maximum concentration employed (IC_{50} ~ 25 μM) (Fig. 8*B*). The other C2 peptides and the scrambled peptide had little effect. The ability of peptide 2228–2240 to inhibit factor Xa generation appeared to be more significant than that in the binding assay. It seemed likely, therefore, that peptide 2228–2240 not only affected interactions between the Gla domain of factor IXa and the C2 domain but also allosterically modulated other reactions. Nevertheless, the findings suggest that interactive site for the Gla domain of factor IXa was located within residues 2228–2240 of the C2 domain.

Effects of peptide 2228–2240 on Factor Xa Generation in the Presence of Phospholipid—Intact C2 and isolated C2 fragments contain phospholipid-binding regions, and to preclude interference by these reactions, our current factor Xa generation

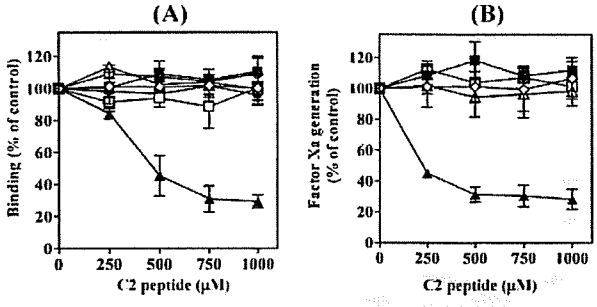

FIGURE 8. **Inhibition of synthetic C2 peptides on EGR-factor IXa binding to rC2 and on factor Xa generation in the absence of phospholipid.** *A*, EGR-factor IXa binding to rC2. Various amounts of synthetic C2 peptide were preincubated with 100 nM EGR-factor IXa for 2 h at 37 °C, prior to the addition to immobilized rC2 (200 nM) in an ELISA-based assay. Absorbance values for the EGR-factor IXa binding to rC2 in the absence of competitor represent the 100% level. The percentage of EGR-factor IXa binding was plotted as a function of peptide concentration. *B*, factor Xa generation in the absence of phospholipid. Various amounts of C2 peptide were preincubated with 5 nM factor IXa for 2 h at 37 °C, and factor Xa generation was initiated with the addition of thrombin-activated factor VIIIa (200 nM) and 1 μM factor X. The initial rate of factor Xa generated in the absence of competitor (100% level) was 0.83 ± 0.01 nM/min. Initial rates of factor Xa generation were plotted as a function of C2 peptide concentration. *Open circles*, peptide 2182–2195; *closed circles*, peptide 2192–2204; *open squares*, peptide 2201–2213; *closed squares*, peptide 2210–2222; *open triangles*, peptide 2219–2231; *closed triangles*, peptide 2228–2240; *open diamonds*, peptide 2237–2249. Experiments were performed at least three separate times, and average ± S.D. values are shown.

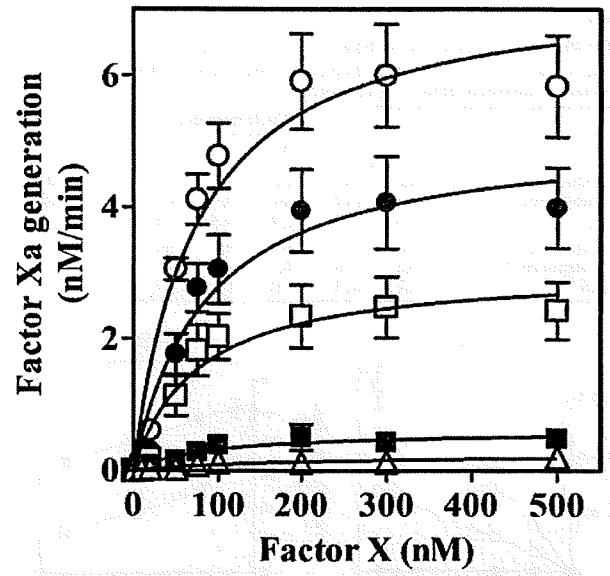

FIGURE 9. **Effect of peptide 2228–2240 on factor Xa generation in the presence of phospholipid.** Factor IXa (0.5 nM) was preincubated with 0 μM (*open circles*), 2.5 μM (*closed circles*), 5 μM (*open squares*), 10 μM (*closed squares*), and 15 μM (*open triangle*) of peptide 2228–2240 for 2 h at 37 °C. Factor Xa generation was initiated by the addition of thrombin-activated factor VIIIa (30 nM) and various concentrations of factor X (0–500 nM) in the presence of phospholipid vesicles (20 μM). Initial rates of factor Xa generation were plotted as a function of factor X concentration and fitted to the Michaelis-Menten equation by nonlinear least squares regression. Experiments were performed at least three separate times, and average ± S.D. values are shown. The V_{max} values in the presence of 0, 2.5, 5, and 10 μM peptide were 7.42 ± 0.85, 5.15 ± 0.73, 3.07 ± 0.49, and 0.61 ± 0.12 nM/min, respectively. The K_m values were 72.9 ± 25.5, 84.8 ± 34.9, 75.0 ± 36.0, and 89.6 ± 51.3 nM, respectively. The kinetic parameters in the presence of 15 μM peptide could not be determined because of very low values.

assays were performed in the absence of phospholipid. Crystal structure analysis has demonstrated that binding of the C2 domain to phospholipid membranes involves three hydrophobic "feet" containing residues Met^{2199}/Phe^{2200}, Val^{2223}, and Leu^{2251}/Leu^{2252} and four basic residues, Arg^{2215}, Arg^{2220}, Lys^{2227}, and Lys^{2249} (35, 36). The factor IXa-interactive site that we have identified within residues 2228–2240 appears, therefore, to be in close proximity to, but not likely to be overlapping, the phospholipid-binding region. In support of this contention, we found that binding of factor VIII and factor IXa to phosphatidylserine was not significantly inhibited by peptide 2228–2240 (data not shown). Nevertheless, to further examine the physiological role of peptide 2228–2240 binding to the Gla domain of factor IXa, factor Xa generation was measured in the presence of factor VIIIa and phospholipid. Factor VIII (30 nM) was activated by thrombin and incubated with factor IXa (0.5 nM)/peptide 2228–2240 mixtures together with various concentrations of factor X in the presence of phospholipid (20 μM). Since rC2-factor IXa interaction was optimal at relatively low concentrations of Ca^{2+} (~1 mM), under these circumstances, the V_{max} was ~20-fold lower than that previously reported (31). Nevertheless, in the presence of peptide 2228–2240, the K_m value remained unchanged, whereas the V_{max} was decreased, dependent on the concentration of the peptide (Fig. 9). Factor Xa generation was completely inhibited (>95%) in the presence of 15 μM peptide. These results suggested that peptide 2228–2240 inhibited factor Xa generation on phospholipid micelles by noncompetitive inhibitory mechanisms. Furthermore, peptide 2228–2240 did not affect factor Xa generation using GDless factor IXa in place of factor IXa in these assays (data not shown), again indicating that peptide 2228–2240 specifically bound to the Gla domain of factor IXa but did not moderate interactions between factor VIIIa and factor X.

DISCUSSION

The enzyme factor IXa and its cofactor factor VIIIa are assembled on phospholipid membranes for the activation of factor X. In previous reports, factor IXa recognition sites were identified within the A2 and A3 domains of factor VIIIa. In the A2 domain, the extended surface, centered on residues 484–509 (16), 558–565 (17), and 708–717 (18), appeared to interact with the factor IXa with weak affinity (~300 nM) (15). In contrast, in the A3 domain, the light chain, including residues 1804–1818 (20), interacted with the protease with high affinity (~15 nM) (19). The structural model of factor VIIIa-factor IXa on phospholipid membranes reported by Blostein *et al.* (21) proposed that the C2 domain of factor VIIIa and the Gla domain of factor IXa bound to phospholipid would be in close proximity, suggesting that both domains might bind to each other. In the present study, we show for the first time that the residues 2228–2240 in the C2 domain and the Gla domain of factor IXa bind to each other.

This conclusion is based on several novel findings using the established models. (i) Direct binding studies demonstrated that active site-modified EGR-factor IXa bound to the C2 domain with mild affinity (~100 nM), whereas GDless EGR-factor IXa failed to bind. In addition, mAb IXa-GD, recognizing the Gla domain of factor IXa, blocked C2-factor IXa interaction. (ii) A factor Xa generation assay without phospholipid showed that rC2 and mAb IXa-GD inhibited factor IXa-medi-

ated factor X activation in the presence of factor VIIIa. (iii) A C2-(2182–2259) fragment, derived from V8 protease-cleaved rC2, directly bound to EGR-factor IXa and inhibited factor Xa generation, whereas the C2-(2260–2322) did not bind. (iv) Competitive assays, using overlapping synthetic peptides encompassing residues 2182–2259, showed that peptide 2228–2240 significantly inhibited both factor IXa binding and factor Xa generation, independently of phospholipid. These data identified amino acid residues 2228–2240 within the C2 domain as essential for factor IXa docking.

In the present study, we utilized EGR-factor IXa, a catalytically inactive derivative of factor IXa, in direct binding experiments. Modified factor IXa prepared with EGR-ck is well known to minimize enzyme-catalyzed degradation, but conformational changes and/or steric hindrance due to incorporation of EGR-ck into the active site of factor IXa may cause difficulties. Nevertheless, Lenting *et al.* (19) reported that thrombin-cleaved factor VIII light chain bound to modified factor IXa with high affinity (~15 nM), and we also analyzed direct binding of the C2 domain using untreated factor IXa and EGR-factor IXa. Binding patterns were similar using active factor IXa and EGR-factor IXa (data not shown), suggesting that any potential effects of conformational changes and/or steric hindrance induced by EGR-ck were minimal. The results also indicated that the C2 domain does not participate in docking to the active site pocket of factor IXa.

We obtained direct evidence for a restricted factor IXa-interactive site in the C2 domain using solvent-accessible surface area analysis with overlapping peptides encompassing residues 2182–2259. The sequence 2228–2240 appeared to be specific for this interaction, and a scrambled peptide confirmed this specificity. The peptide 2228–2240 did not affect factor VIII binding to phospholipid, however, in keeping with an earlier study using similar C2 peptides (7). Our observations add significantly to understanding the nature of the factor Xase complex involving factor IXa and the C2 domain of factor VIII. Our suggestion that this region is not related to phospholipid binding by experiments using peptide can be supported by the following reasons.

First, based on the ability of synthetic peptides encompassing residues 2303–2332 in C2 to inhibit factor VIII-phospholipid binding, a major site was previously located within this region (7). In addition, earlier elegant examination of the 1.5 Å x-ray structure of the C2 domain revealed the presence of three hydrophobic "feet" (Met^{2199}/Phe^{2200}, Val^{2223}, and Leu^{2251}/Leu^{2252}) that penetrate the membrane and four basic residues (Arg^{2215}, Arg^{2220}, Lys^{2227}, and Lys^{2249}) that lie underneath the "feet" and stabilize binding by electrostatic interaction with phospholipid (35, 36). These findings show that the 2228–2240 region in C2 is in close proximity to, but is not likely to overlap, the phospholipid-binding region. Second, The interaction between factor IXa and thrombin-cleaved factor VIII light chain, lacking the acidic region of the A3 domain involved in high affinity VWF binding, was not affected by the presence of VWF (19). Our present study also showed that the C2-factor IXa interaction was not affected by VWF (data not shown). Since the C2 domain is involved in VWF binding at a site that overlaps the phospholipid-binding site (8, 9), the 2228–2240 region does not overlap this site. Last, factor VIIIa contacts with residue Phe^{25} and/or Val^{46} of the Gla domain of factor IXa but not with the membrane-binding ω loop (residues 1–11) (21). Furthermore, a naturally occurring mutation (G12R) within the Gla domain is associated with reduced activity of the factor Xase complex but does not affect phospholipid binding (37). These results are consistent with the view that interaction between the Gla domain and the C2 domain is not dependent on phospholipid binding. Taken together, our findings imply that interactions between both domains facilitate a tight ternary complex with phospholipid.

Binding of C2 to the Gla domain of factor IXa was governed by electrostatic and/or calcium-dependent interactions. This mechanism was similar to that observed between the light chain of factor VIII and factor IXa (19). Furthermore, peptide 2228–2240 significantly inhibited (>95%) factor Xa generation in the presence of phospholipid through noncompetitive inhibitory mechanisms, similar to those observed using peptide 1804–1818, previously reported as a factor IXa-binding site in A3. These data strongly indicated that the properties of both interactions were common and that both peptides inhibited the enzyme activity of factor IXa by binding at a site distinct from the substrate binding pocket. Of interest, the binding affinity of C2 for factor IXa (~100 nM) was ~7-fold lower than that of the light chain (~15 nM). In the absence of phospholipid, the inhibitory effect of peptide 2228–2240 on C2-factor IXa interaction was not significantly different from that of peptide 1804–1818 on light chain-factor IXa interaction. In the presence of phospholipid, however, peptide 2228–2240 appeared to inhibit factor Xa generation more strongly than peptide 1804–1818 (IC_{50} ~ 5 and ~600 μM, respectively). The binding affinity of the A3 domain for factor IXa is not known; nevertheless, the high affinity of the light chain appears to make an essential contribution to reactions involving not only the A3 domain but also the C2 domain. Furthermore, the data indicate that peptide 2228–2240 predominantly participates in factor IXa docking for catalyzing the activity of the factor Xase enzyme.

Recently, two groups have reported the intermediate resolution x-ray crystallographic structure of B-domainless factor VIII (38, 39). Factor IXa-interactive sites within factor VIII based on crystal structure reveal that residues 558–565 and 708–717 in A2 and 1804–1818 in A3 are located on one face of factor VIII, whereas residues 484–509 in A2 and our identified 2228–2240 in C2 are located on another face. Ngo *et al.* (39) have constructed a model of the factor VIIIa-factor IXa complex with x-ray crystal structure of human factor VIII and porcine factor IXa backbone with the following constraints. Residues 558–565, 708–717, and 1804–1818 of factor VIIIa interact with the residues 330–339, residues 301–303, and the putative binding region, including EGF domains (Tyr^{69} and Asn^{92}) and Gla domain (Phe^{25}) of factor IXa, respectively. Although this differed from our data in the binding site of C2 for the Gla domain, a factor IXa-interactive site comprising residues 2228–2240 in C2 is unlikely to contact the Gla domain simultaneously according to this model. This discrepancy may be due to conformational change of the C2 domain. Conformational changes in C2 of factor VIIIa upon removal of the NH_2 terminus of the light chain (residues 1649–1689) (40) probably

leads to enhancement of the factor VIIIa affinity for phospholipid membrane (41). This may affect the Gla domain binding. In addition, the C2 domain is relatively loosely docked to the remainder of factor VIII molecules (38, 39); consequently, the position of this domain within active form factor VIIIa on the phospholipid surface may change easily. These findings can be supported by the case of residues 484–509 in A2. The model proposed by Ngo showed that this region did not interact with factor IXa despite the factor IXa-interactive site. Bajaj *et al.* (42) also demonstrated that residues 484–509 in A2 were not in close proximity to one face consisting of residues 558–565, 708–717, and 1804–1818 and did not contact factor IXa. Furthermore, Stoilova-McPhie *et al.* (43) found that it was unable to modify the factor VIII-factor IXa binding model, including the 484–509 region. The following possibilities are raised for this reason: the conformational change in A2 upon binding of the catalytic domain of factor IXa and different A2 arrangement between unactive form factor VIII and active form factor VIIIa. Therefore, it is not so surprising that the 2228–2240 region in factor VIIIa interacts with factor IXa Gla domain.

An earlier report by Nogami *et al.* (11) demonstrated that residues 2253–2270 within the C2 domain of factor VIII contribute to a unique factor Xa-interactive site within the light chain that promotes factor Xa docking during cofactor activation and cleavage of the light chain at Arg^{1689}. Binding of factor Xa to the C2 domain was independent of binding to phospholipid or VWF, indicative of a distinct factor Xa-binding site in the C2 domain. This binding was remarkably similar to that of the C2-factor IXa interaction observed in this study. In addition, interaction between the light chain of factor VIIIa and factor IXa was not inhibited by active site-modified factor Xa (19). However, the C2-factor IXa interaction was not inhibited by anti-C2 mAb ESH8 (data not shown), which recognizes residues 2248–2285 and inhibits the factor VIII-factor Xa interaction (11). These findings suggest that the factor IXa-interactive site in the C2 domain does not overlap the factor VIII-Xa interactive site.

Comparisons of amino acid sequences among human, porcine, murine, and canine factor VIII molecules indicate that residues 2228–2240 within the C2 domain are well conserved, in keeping with the suggestion that this region could be fundamental for interaction with the Gla domain of factor IXa (44–46). This region appears to be unique, and the specific sequence of residues is distinct from those of the factor IXa-interactive sites within the A2 and A3 domains of factor VIIIa (16–18, 20). Naturally occurring mutations of residues 2228–2240 (W2229C, W2229S, Q2231H, V2232A/E, and M2238V) have been reported in the hemophilia A data base (HAMSTeRS), and are seen in mild/moderate hemophilia A. It is tempting to speculate that the pathogenic mechanism for these point mutations might be associated with dysfunctional blood coagulation by moderating interactions between the C2 domain of factor VIIIa and the Gla domain of factor IXa. Furthermore, substitutions at Trp^{2229} to Cys and Val^{2232} to Ala are related to the development of inhibitors (47, 48), consistent with our suggestion that the 2228–2240 region in C2 is surface-exposed and influences antigenicity.

In conclusion, we provide the first evidence for an essential role of the association between the 2228–2240 region of the C2 domain and the Gla domain of factor IXa in the factor Xase complex. Further studies using site-directed mutagenesis are warranted to further clarify the functional role of residues 2228–2240 in the C2 domain.

Acknowledgment—We thank Dr. J. C. Giddings for helpful suggestions.

REFERENCES

1. Toole, J. J., Knopf, J. L., Wozney, J. M., Sultzman, L. A., Buecker, J. L., Pittman, D. D., Kaufman, R. J., Brown, E., Shoemaker, C., Orr, E. C., Amphlett, G. W., Foster, W. B., Coe, M. L., Knudson, G. J., Fass, D. N., and Hewick, R. M. (1984) *Nature* **312,** 342–347
2. Wood, W. I., Capon, D. J., Simonsen, C. C., Eaton, D. L., Gitschier, J., Keyt, B., Seeburg, P. H., Smith, D. H., Hollingshead, P., Wion, K. L., Delwart, E., Tuddenham, E. G. D., Vehar, G. A., and Lawn, R. M. (1984) *Nature* **312,** 330–337
3. Vehar, G. A., Keyt, B., Eaton, D., Rodriguez, H., O'Brien, D. P., Rotblat, F., Oppermann, H., Keck, R., Wood, W. I., Harkins, R. N., Tuddenham, E. G. D., Lawn, R. M., and Capon, D. J. (1984) *Nature* **312,** 337–342
4. Shima, M., Scandella, D., Yoshioka, A., Nakai, H., Tanaka, I., Kamisue, S., Terada, S., and Fukui, H. (1993) *Thromb. Haemost.* **69,** 240–246
5. Saenko, E. L., Shima, M., Rajalakshmi, K. J., and Scandella, D. (1994) *J. Biol. Chem.* **269,** 11601–11605
6. Shima, M., Nakai, H., Scandella, D., Tanaka, I., Sawamoto, Y., Kamisue, S., Morichika, S., Murakami, T., and Yoshioka, A. (1995) *Br. J. Haematol.* **91,** 714–721
7. Foster, P. A., Fulcher, C. A., Houghten, R. A., and Zimmerman, T. S. (1990) *Blood* **75,** 1999–2004
8. Nogami, K., Shima, M., Nakai, H., Tanaka, I., Suzuki, H., Morichika, S., Shibata, M., Saenko, E. L., Scandella, D., Giddings, J. C., and Yoshioka, A. (1999) *Br. J. Haematol.* **107,** 196–203
9. Nogami, K., Shima, M., Giddings, J. C., Takeyama, M., Tanaka, I., and Yoshioka, A. (2007) *Int. J. Hematol.* **85,** 317–322
10. Nogami, K., Shima, M., Hosokawa, K., Nagata, M., Koide, T., Saenko, E. L., Tanaka, I., Shibata, M., and Yoshioka, A. (2000) *J. Biol. Chem.* **275,** 25774–25780
11. Nogami, K., Shima, M., Hosokawa, K., Suzuki, T., Koide, T., Saenko, E. L., Scandella, D., Shibata, M., Kamisue, S., Tanaka, I., and Yoshioka, A. (1999) *J. Biol. Chem.* **274,** 31000–31007
12. Healey, J. F., Barrow, R. T., Tamim, H. M., Lubin, I. M., Shima, M., Scandella, D., and Lollar, P. (1998) *Blood* **92,** 3701–3709
13. van Dieijen, G., Tans, G., Rosing, J., and Hemker, H. C. (1981) *J. Biol. Chem.* **256,** 3433–3442
14. Schmidt, A. E., and Bajaj, S. P. (2003) *Trends Cardiovasc. Med.* **13,** 39–45
15. Fay, P. J., and Koshibu, K. (1998) *J. Biol. Chem.* **273,** 19049–19054
16. Fay, P. J., and Scandella, D. (1999) *J. Biol. Chem.* **274,** 29826–29830
17. Fay, P. J., Beattie, T., Huggins, C. F., and Regan, L. M. (1994) *J. Biol. Chem.* **269,** 20522–20527
18. Jenkins, P. V., Dill, J. L., Zhou, Q., and Fay, P. J. (2004) *Biochemistry* **43,** 5094–5101
19. Lenting, P. J., Donath, M. J., van Mourik, J. A., and Mertens, K. (1994) *J. Biol. Chem.* **269,** 7150–7155
20. Lenting, P. J., van de Loo, J. W., Donath, M. J., van Mourik, J. A., and Mertens, K. (1996) *J. Biol. Chem.* **271,** 1935–1940
21. Blostein, M. D., Furie, B. C., Rajotte, I., and Furie, B. (2003) *J. Biol. Chem.* **278,** 31297–31302
22. Freedman, S. J., Blostein, M. D., Baleja, J. D., Jacobs, M., Furie, B. C., and Furie, B. (1996) *J. Biol. Chem.* **271,** 16227–16236
23. Sugo, T., Mizuguchi, J., Kamikubo, Y., and Matsuda, M. (1990) *Thromb. Res.* **58,** 603–614
24. Mimuro, J., Mizukami, H., Ono, F., Madoiwa, S., Terao, K., Yoshioka, A., Ozawa, K., and Sakata, Y. (2004) *J. Thromb. Haemost.* **2,** 275–280
25. Morita, T., and Kisiel, W. (1985) *Biochem. Biophys. Res. Commun.* **130,** 841–847
26. Mimms, L. T., Zampighi, G., Nozaki, Y., Tanford, C., and Reynolds, J. A.